INTERNATIONAL JOURNAL FOR NUMERICAL METHODS IN FLUIDS, VOL. 11, 1043–1073 (1990)

AN UPWIND SCHEME FOR THE THREE-DIMENSIONAL BOUNDARY LAYER EQUATIONS

L. J. JOHNSTON*

Aeronautics/Aerospace Department, von Karman Institute for Fluid Dynamics, B-1640 Rhode Saint Genèse, Belgium

SUMMARY

The development of a calculation method to solve the compressible, three-dimensional, turbulent boundary layer equations is described. An implicit finite difference solution procedure is adopted involving local upwinding of convective transport terms. A consistent approach to discretization and linearization is taken by casting all equations in a similar form. The implementation of algebraic, one-equation and two-equation turbulence models is described. An initial validation of the method is made by comparing prediction with measurements in two quasi-three-dimensional boundary layer flows. Some of the more obvious deficiencies in current turbulence-modelling standards for three-dimensional flows are discussed.

KEY WORDS Three-dimensional flows Turbulent boundary layers Numerical methods Finite difference schemes Turbulence modelling

INTRODUCTION

It is now feasible to predict the detailed viscous flow development over three-dimensional surfaces such as wings and bodies by solving the Reynolds-averaged Navier–Stokes equations.[1] However, such calculations are computationally intensive and so are unlikely to be carried out on a routine basis in the near future. For this reason the development of efficient solution methods for the three-dimensional turbulent boundary layer equations continues to receive much attention. When coupled to an inviscid flow solver, such methods provide an economic means of obtaining 'reasonable' predictions of three-dimensional viscous flows, at least in fully attached flow situations. The use of inverse solution procedures to march the boundary layer equations into separated flow regions is an area of current research activity.[2,3]

A EUROVISC workshop was held in Berlin in 1982 to assess the performance of 14 existing calculation methods for three-dimensional turbulent boundary layers. Humphreys and Lindhout[4] give a detailed description of the methods, and the results of the workshop comparisons of predictions are now available.[5] Conclusions drawn from the workshop indicate that satisfactory calculation methods are available for three-dimensional turbulent boundary layers, but that predictions, even for fully attached flows, suffer owing to the current poor state of turbulence modelling for three-dimensional flows. The majority of existing 'production' calculation methods use simple algebraic turbulence models adapted from well established models for two-dimensional flow. However, experiments[6] indicate that this simple-minded approach is inadequate due to the non-isotropic nature of the shear stress vector in three-dimensional flows.

The present paper describes the development of a new calculation method for compressible, three-dimensional, turbulent boundary layer flows. The governing flow equations are solved in

* Present address: Department of Mechanical Engineering, UMIST, PO Box 88, Manchester, M60 1QD, U.K.

0271–2091/90/161043–31$15.50

Received January 1989
Revised January 1990

differential form using finite difference techniques. A space-marching procedure is used whereby the solution is marched away from specified conditions on an initial line, subject to an imposed external flow pressure distribution. The boundary layer equations are thus solved in direct mode and the solution is forbidden to enter separated flow regions. The method can, however, map out the boundaries of such regions.

A particular consideration in the development of the present method has been the establishment of consistent discretization and linearization procedures for the mean-flow momentum and energy equations. These procedures can be readily extended to the transport equations used in more sophisticated turbulence models. The paper discusses the implementation of representative zero-, one- and two-equation turbulence models. The performance of the calculation method (and the relative performance of the various turbulence models) is assessed by comparison with some of the available experimental data on three-dimensional turbulent boundary layers. It is intended that this assessment of some 'standard' turbulence models be used as the starting point for investigations aimed at improving the current state of turbulence modelling for three-dimensional flows.

The present calculation method has been developed on the basis of experience gained in the development and use of two earlier methods. The first method[7] was developed at the Aircraft Research Association Ltd. in Bedford, U.K. under contract to the U.K. Ministry of Defence. More recently, a substantially improved method[8,9] has been developed from which the present calculation method is evolved. The detailed differences between these various methods will be discussed below.

MEAN-FLOW EQUATIONS

The problem to be considered is the turbulent boundary layer development over a three-dimensional surface. Figure 1 shows the non-orthogonal surface co-ordinate system in which the boundary layer equations are to be solved. X and Y are the surface co-ordinates with a local angle θ between them, and the third co-ordinate Z is normal to the surface. The governing mean-flow equations for a steady, compressible, three-dimensional turbulent flow are

continuity

$$\frac{\partial(\rho U h_2 \sin\theta)}{\partial X}+\frac{\partial(\rho V h_1 \sin\theta)}{\partial Y}+\frac{\partial(\rho W h_1 h_2 \sin\theta)}{\partial Z}=0, \tag{1}$$

X-momentum

$$\frac{\rho U}{h_1}\frac{\partial U}{\partial X}+\frac{\rho V}{h_2}\frac{\partial U}{\partial Y}+\rho W\frac{\partial U}{\partial Z}-k_1\cot\theta\,\rho U^2+k_2\operatorname{cosec}\theta\,\rho V^2+k_{12}\rho U V$$
$$=\frac{\partial}{\partial Z}\left(\frac{\mu+\mu_t}{R}\frac{\partial U}{\partial Z}\right)-\frac{\operatorname{cosec}^2\theta}{h_1}\frac{\partial P}{\partial X}+\frac{\cot\theta\operatorname{cosec}\theta}{h_2}\frac{\partial P}{\partial Y}, \tag{2}$$

Y-momentum

$$\frac{\rho U}{h_1}\frac{\partial V}{\partial X}+\frac{\rho V}{h_2}\frac{\partial V}{\partial Y}+\rho W\frac{\partial V}{\partial Z}+k_1\operatorname{cosec}\theta\,\rho U^2-k_2\cot\theta\,\rho V^2+k_{21}\rho U V$$
$$=\frac{\partial}{\partial Z}\left(\frac{\mu+\mu_t}{R}\frac{\partial V}{\partial Z}\right)+\frac{\cot\theta\operatorname{cosec}\theta}{h_1}\frac{\partial P}{\partial X}-\frac{\operatorname{cosec}^2\theta}{h_2}\frac{\partial P}{\partial Y}, \tag{3}$$

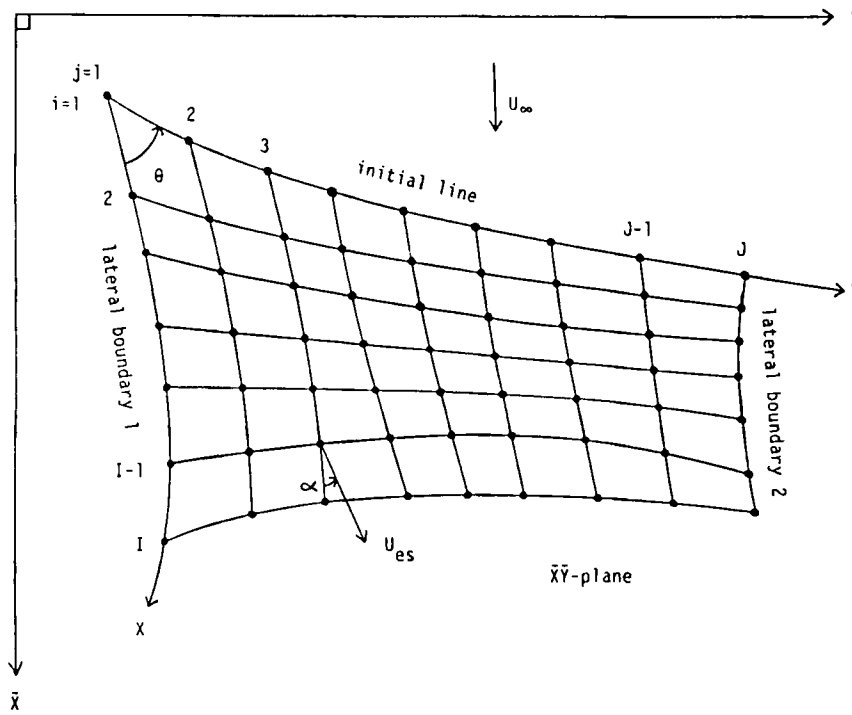

Figure 1. Non-orthogonal surface co-ordinate system

Z-momentum

$$\frac{\partial P}{\partial Z}=0, \tag{4}$$

energy

$$\frac{\rho U}{h_1}\frac{\partial H}{\partial X}+\frac{\rho V}{h_2}\frac{\partial H}{\partial Y}+\rho W\frac{\partial H}{\partial Z}=\frac{\partial}{\partial Z}\left[\frac{1}{R}\left(\frac{\mu}{Pr}+\frac{\mu_t}{Pr_t}\right)\frac{\partial H}{\partial Z}+\frac{\mu}{R}\left(1-\frac{1}{Pr}\right)\frac{\partial(U_t^2/2)}{\partial Z}\right], \tag{5}$$

equation of state

$$\rho=\frac{\gamma P}{(\gamma-1)(H-\frac{1}{2}U_t^2)}, \tag{6}$$

where U, V, W, H, ρ and P are the physical velocity components in the three co-ordinate directions, total enthalpy, density and static pressure respectively. U_t is the total mean velocity

$$U_t^2=U^2+V^2+2\cos\theta\, UV, \tag{7}$$

whose value at the edge of the boundary layer will be denoted by U_{es}. The local laminar viscosity μ is given by Sutherland's law and the Reynolds shear stress terms have been modelled by an isotropic eddy viscosity μ_t. The laminar and turbulent Prandtl numbers Pr and Pr_t are assumed to have constant values of 0·72 and 0·9 respectively. Finally, γ is the ratio of specific heats, equal to 1·4 for air.

The above equations are written in terms of mass-weighted average variables and are in non-dimensional form (as are all subsequent equations). Variables are scaled with the free stream velocity, density, viscosity and a length scale, which can be combined to give the reference Reynolds number R. The various metric quantities relating to the surface co-ordinate system are defined in the Appendix. The boundary conditions for the mean-flow equations are

$$U=V=W=0, \qquad H=H_w \quad \text{at } Z=0,$$
$$U=U_e, \quad V=V_e, \quad H=H_e \quad \text{as } Z\to\infty, \tag{8}$$

where subscripts 'w' and 'e' refer to conditions at the surface and boundary layer edge respectively.

Equations (2), (3) and (5) are to be solved for U, V and H, and the three equations can be written in the following similar form:

$$\rho U\left(\frac{1}{h_1}\frac{\partial\alpha_m}{\partial X}+A_m\alpha_m\right)+\rho V\left(\frac{1}{h_2}\frac{\partial\alpha_m}{\partial Y}+B_m\alpha_m\right)+\rho W\frac{\partial\alpha_m}{\partial Z}+\rho C_m\alpha_m-\frac{\partial}{\partial Z}\left(b_m\frac{\partial\alpha_m}{\partial Z}\right)=\rho R_m, \tag{9}$$

where

$m=1$ (X-momentum equation)

$$\alpha_1\equiv U,$$
$$A_1=-k_1\cot\theta, \qquad B_1=k_{12}, \qquad C_1=0, \qquad b_1=(\mu+\mu_t)/R,$$
$$R_1=-V^2k_2\operatorname{cosec}\theta-\frac{\operatorname{cosec}^2\theta}{\rho h_1}\frac{\partial P}{\partial X}+\frac{\cot\theta\operatorname{cosec}\theta}{\rho h_2}\frac{\partial P}{\partial Y},$$

$m=2$ (Y-momentum equation)

$$\alpha_2\equiv V,$$
$$A_2=k_{21}, \qquad B_2=-k_2\cot\theta, \qquad C_2=0, \qquad b_2=(\mu+\mu_t)/R,$$
$$R_2=-U^2k_1\operatorname{cosec}\theta+\frac{\cot\theta\operatorname{cosec}\theta}{\rho h_1}\frac{\partial P}{\partial X}-\frac{\operatorname{cosec}^2\theta}{\rho h_2}\frac{\partial P}{\partial Y},$$

$m=3$ (energy equation)

$$\alpha_3\equiv H,$$
$$A_3=0, \qquad B_3=0, \qquad C_3=0, \qquad b_3=\frac{1}{R}\left(\frac{\mu}{Pr}+\frac{\mu_t}{Pr_t}\right),$$
$$R_3=\frac{1}{\rho}\frac{\partial}{\partial Z}\left[\frac{\mu}{R}\left(1-\frac{1}{Pr}\right)\frac{\partial(U_t^2/2)}{\partial Z}\right].$$

A uniform computational grid is to be used in the direction normal to the surface and it is convenient to introduce the following scaled co-ordinates:

$$x=X, \qquad y=Y, \qquad z=\frac{\tanh\left[\left(\frac{1}{\theta_k}\int_0^Z\rho\,dZ\right)^{1/2}\Big/A\right]}{\tanh(B)}, \tag{10}$$

where A and B are constants and θ_k is a total momentum thickness

$$\theta_k = \int_0^\infty [\rho U_t (U_{es} - U_t)/\rho_e U_{es}^2] \mathrm{d}Z. \tag{11}$$

The above scaling of the normal co-ordinate Z, when used with a uniform computational grid in the transformed co-ordinate z, concentrates points close to the surface and enables an accurate evaluation of the skin friction. The scaling with θ_k removes most of the boundary layer growth in computational space and introduces a stretching function parameter λ into the mean-flow equations,

$$\lambda = \frac{2A^2 \tanh(B) \tanh^{-1}[z \tanh(B)]}{1 - [z \tanh(B)]^2}. \tag{12}$$

A two-component streamfunction (Ψ, Φ) can be defined,

$$\rho U h_2 \sin\theta = \frac{\partial \Psi}{\partial Z}, \qquad \rho V h_1 \sin\theta = \frac{\partial \Phi}{\partial Z}, \qquad \rho W h_1 h_2 \sin\theta = -\left(\frac{\partial \Psi}{\partial X} + \frac{\partial \Phi}{\partial Y}\right), \tag{13}$$

which satisfies the continuity equation exactly, and so equation (1) can be replaced by two equations for Ψ and Φ. The transformed mean-flow equations are

streamfunctions

$$\lambda U \theta_k h_2 \sin\theta = \frac{\partial \Psi}{\partial z}, \qquad \lambda V \theta_k h_1 \sin\theta = \frac{\partial \Phi}{\partial z}, \tag{14}$$

α_m-equation

$$U\left(\frac{1}{h_1}\frac{\partial \alpha_m}{\partial x} + A_m \alpha_m\right) + V\left(\frac{1}{h_2}\frac{\partial \alpha_m}{\partial y} + B_m \alpha_m\right) + \frac{w}{\lambda}\frac{\partial \alpha_m}{\partial z} + C_m \alpha_m - \frac{1}{\lambda \theta_k}\frac{\partial}{\partial z}\left(\frac{\rho b_m}{\lambda \theta_k}\frac{\partial \alpha_m}{\partial z}\right) = R_m, \tag{15}$$

where w is a scaled mean velocity normal to the surface,

$$w = -\frac{1}{\theta_k h_1 h_2 \sin\theta}\left(\frac{\partial \Psi}{\partial x} + \frac{\partial \Phi}{\partial y}\right), \tag{16}$$

and the boundary conditions become

$$U = V = \Psi = \Phi = 0, \quad H = H_w \quad \text{at } z = 0,$$
$$U = U_e, \quad V = V_e, \quad H = H_e \quad \text{as } z \to \infty. \tag{17}$$

Initial conditions for the calculation must be specified on an $x =$ constant line. The solution is marched downstream from this initial line, subject to the external flow and boundary conditions. The external flow is supplied to the calculation in terms of the surface pressure distribution. The outer boundary conditions on U, V and H are obtained by solving the two-dimensional Euler equations for the inviscid flow external to the boundary layer. This is done by setting all terms involving $\partial/\partial z$ derivatives to zero in equation (15). Alternatively, the external flow conditions may be supplied to the method by an independent inviscid flow solver. Additional boundary conditions are needed if there is any flow into the computational domain through the two lateral boundaries. The set of mean-flow equations is closed once a turbulence model for the eddy viscosity μ_t is specified.

DISCRETIZATION OF α_m-EQUATION

The transformed momentum and energy equations in the similar form of equation (15) are coupled and non-linear. The present method employs implicit finite difference formulae in the y- and z-directions to approximate the equations, and so the solution procedure on a given yz-plane is iterative. Following Johnston,[8,9] equation (15) is solved for α_m, the equation being linearized by evaluating all other variables at the previous iteration level. The three equations ($m = 1, 2, 3$) are now decoupled and can be solved in sequence for U, V and H respectively. This approach can be contrasted with that in the original method of Johnston,[7] which uses a Newton linearization procedure. Also, certain mean-flow variables are scaled with their values at the edge of the boundary layer. The resulting set of discretized equations are more complex than those of the present method, since each of equations (2), (3) and (5) is treated in a slightly different manner. The present approach to discretization and linearization is much more consistent and does not appear to increase the number of iterations required to converge the solution.

As shown in Figure 1, the continuous solution of the mean-flow equations in the computational domain is approximated by discrete solutions at a finite number of points. A regular Cartesian grid is used in transformed space, there being (I, J, K) grid points with spacings $(\Delta x, \Delta y, \Delta z)$ in the three co-ordinate directions (x, y, z). For convenience, $\Delta x = \Delta y = \Delta z = 1$, the spacings between grid points in physical space being taken care of in the determination of the surface grid metric quantities (see Appendix) and the normal co-ordinate transformation, equation (10). Suffices (i, j, k) are used to denote a variable evaluated at a particular grid point.

The discrete form of equation (15) for α_m is centred at (i, j, k), and the various finite difference formulae used to approximate the convective transport terms are given below. For clarity, the suffix m is dropped from α_m in this section, and suffices on the right-hand side of an expression are suppressed if their values are unchanged from those on the left-hand side. Finally, a prime on a quantity denotes a variable evaluated at the previous iteration level.

$U(\partial\alpha/\partial x)$

The solution of the mean-flow equations is marched downstream in the x-direction, subject to the imposed pressure distribution external to the boundary layer. Such a direct mode calculation will break down if reverse flow occurs in the marching direction. The method therefore assumes $U > 0$, and the following approximation to this convective transport term is used:

$$\left(U\frac{\partial\alpha}{\partial x}\right)_{i,j,k} = U'_i(\beta_1\alpha_i + \beta_2\alpha_{i-1} + \beta_3\alpha_{i-2})/\Delta x, \tag{18}$$

where the coefficients β_1 to β_3 are given in Table I. Note that for $i > 2$ a second-order-accurate one-sided formula is used to discretize $\partial\alpha/\partial x$. At $i = 2$ there is no station corresponding to $i-2$, since $i-1$ is the initial station, and so a first-order-accurate formula is used. This approach is

Table I. Coefficients for discretization of x-derivatives in convective transport terms, equation (18)

i	β_1	β_2	β_3
2	1	−1	0
>2	3/2	−4/2	1/2

permissible since an initial value problem is being solved and the solution further downstream should not be too dependent on the starting conditions.

The earlier method of Johnston[8,9] uses a Crank–Nicholson scheme at all x-stations to discretize $\partial\alpha/\partial x$, with equation (15) being centred at $(i-1/2, j, k)$. Experience with this earlier method indicates that the use of the Crank–Nicholson scheme can lead to an oscillatory behaviour of quantities such as the skin friction and limiting surface streamline angle (these are sensitive parameters since they are obtained by numerical differentiation). This behaviour occurs primarily when marching away from the initial data, when the mean-flow equations are solved in conjunction with a two-equation turbulence model. The present use of an upwind scheme, equation (18), suppresses this tendency.

The procedure followed if, during the course of a calculation, U becomes negative at any point across the boundary layer is discussed in the next section.

$V(\partial\alpha/\partial y)$

The treatment of this convective transport term is the key to the successful development of a practical calculation method. The way in which $\partial\alpha/\partial y$ can be approximated is related to the numerical scheme used to advance the solution from $i-1$ to i. The majority of existing methods[4,10] march the solution in the positive y-direction (see Figure 1), converging the solution at station (i, j) before going on to station $(i, j+1)$. This approach is satisfactory provided that $V \geqslant 0$ for all points across the boundary layer at station (i, j). Otherwise, the solution at (i, j) will be dependent upon information at station $(i, j+1)$, which is not available. In such circumstances it is usual to evaluate $\partial\alpha/\partial y$ at $(i-1, j)$ for any points at (i, j) where $V<0$. This approach is subject to a stability restriction that requires the streamline through (i, j, k) to intersect the yz-plane through x_{i-1} between y_j and y_{j+1}. Lindhout *et al.*[11] take an alternative approach which involves marching the solution in both the positive and negative y-directions, the direction being determined by the sign of the maximum local value of V across the boundary layer.

A more consistent approach is to remove the stability restriction altogether by using an implicit solution procedure in both the y- and z-directions. In this way the solution over the whole yz-plane through x_i is obtained simultaneously. Nash and Scruggs[12] and Tassa *et al.*[13] both follow this approach, employing alternating direction implicit (ADI) solution procedures. The present method adopts the technique devised by Johnston[8,9] whereby the solution is obtained simultaneously over a yz-plane using a numerical scheme which marches in the positive y-direction only. The marching from $j=1$ to J is carried out at each iteration of the solution procedure. By this means the information at $(i, j+1)$, required to evaluate $\partial\alpha/\partial y$ when $V<0$, is always available (at the previous iteration level).

The term $V(\partial\alpha/\partial y)$ is approximated using a general five-node computational molecule:[8,9]

$$\left(V\frac{\partial\alpha}{\partial y}\right)_{i,j,k} = \left(\frac{V_j'+|V_j'|}{2}\right)\left(\frac{\gamma_1\alpha_{j+1}'+\gamma_2\alpha_j+\gamma_3\alpha_{j-1}+\gamma_4\alpha_{j-2}}{2\Delta y}\right) + \left(\frac{V_j'-|V_j'|}{2}\right)\left(\frac{\gamma_5\alpha_{j+2}'+\gamma_6\alpha_{j+1}'+\gamma_7\alpha_j+\gamma_8\alpha_{j-1}}{2\Delta y}\right). \tag{19}$$

The coefficients γ_1 to γ_8 can be chosen to give various discrete approximations to $\partial\alpha/\partial y$. For example, Table II gives the coefficients appropriate to a second-order-accurate upwind scheme (the default scheme of the method) and the QUICK scheme of Leonard.[14] Both of these schemes have an upwind bias, and the formulation of equation (19) allows the bias to be determined by the sign of the local mean convection velocity V.

Table II. Coefficients for discretization of y-derivatives in convective transport terms, equation (19)

j	γ_1	γ_2	γ_3	γ_4	γ_5	γ_6	γ_7	γ_8
(a) *Second-order upwind scheme*								
1	0	0	0	0	−1	4	−3	0
2	1	0	−1	0	−1	4	−3	0
$2<j<J-1$	0	3	−4	1	−1	4	−3	0
$J-1$	0	3	−4	1	0	1	0	−1
J	0	3	−4	1	0	0	0	0
(b) *QUICK scheme*								
1	0	0	0	0	−1	4	−3	0
2	1	0	−1	0	−1/3	2	−1	−2/3
$2<j<J-1$	2/3	1	−2	1/3	−1/3	2	−1	−2/3
$J-1$	2/3	1	−2	1/3	0	1	0	−1
J	0	3	−4	1	0	0	0	0

The standard second-order-accurate upwind or QUICK schemes can be used at all stations in the range $2<j<J-1$. Table II indicates that the schemes can also be used at $j=2$ and $j=J-1$ if the sign of V allows it, otherwise a centre difference scheme is adopted.

There will be flow into the computational domain through the lateral boundaries if $V>0$ at $j=1$ or $V<0$ at $j=J$. In such circumstances the default action of the method is to set $\partial\alpha/\partial y$ to zero at grid points where there is flow into the computational domain, with the second-order-accurate upwind scheme being used for all grid points with outflow. Alternatively, one or both of the lateral boundaries can be designated a plane of symmetry on which the appropriate equations are solved; see Reference 15 for details. This approach would be taken to calculate the flow development on a body at incidence if both the body and flow have a plane of symmetry. A final alternative is a body of general shape, or for a symmetric body with a free stream flow involving both incidence and side slip. Periodic boundary conditions would be applied at the two lateral boundaries in such a case, the boundaries being purely notional. The standard differencing schemes given in Table II for $2<j<J-1$ can then be used for $j=1$ to J.

$w(\partial\alpha/\partial z)$

This term represents convective transport across the boundary layer. A centre difference discretization of $\partial\alpha/\partial z$ can induce 'wiggles' in the profile of α at the edge of the boundary layer. The wiggles occur when $w<0$ and appear to be due to the scaling of the normal co-ordinate with the local total momentum thickness, equation (10). Therefore a centre difference formula is used only if $w\geqslant 0$, and a one-sided formula is used if the convective transport across the boundary layer is directed towards the surface:

$$\left(w\frac{\partial\alpha}{\partial z}\right)_{i,j,k}=\left(\frac{w'_k+|w'_k|}{2}\right)\left(\frac{\alpha_{k+1}-\alpha_{k-1}}{2\Delta z}\right)+\left(\frac{w'_k-|w'_k|}{2}\right)\left(\frac{-3\alpha_k+4\alpha_{k+1}-\alpha'_{k+2}}{2\Delta z}\right). \tag{20}$$

SOLUTION PROCEDURE

After following the linearization and discretization procedures described in the previous section, the three mean-flow equations represented by equation (15) can be solved for U, V and H

respectively. The solution procedure adopted is as follows (again, subscript m on α_m has been dropped for clarity). Define the correction to $\alpha_{i,j,k}$ as

$$\alpha_{i,j,k} = \alpha'_{i,j,k} + \delta\alpha_k, \tag{21}$$

where, as usual, the prime indicates a variable evaluated at the previous iteration level. The discretized version of equation (15) can then be written in the form

$$A_k\delta\alpha_{k-1} + B_k\delta\alpha_k + C_k\delta\alpha_{k+1} = D_k \quad \text{for } 1 < k < K. \tag{22}$$

This tridiagonal system of equations is completed by the discrete versions of the surface boundary condition at $k=1$ and the outer boundary condition at $k=K$, equation (17).

The calculation method in its present form is applicable to fully turbulent flow only. Therefore starting profiles must be provided for the mean-flow quantities at each y-station on the initial line $i=1$ (see Figure 1). The solution is then marched in the x-direction, away from these starting conditions. The initial mean-velocity profile at each y-station is defined in two parts, with components U_s in the local external streamline direction and U_c in the crossflow direction, orthogonal to U_s. The streamwise profile is defined in analytic form as a combined law-of-the-wall/law-of-the-wake, together with a near-wall damping function. The crossflow mean-velocity component is related to the streamwise component via the profile family of Mager. An extension of the Crocco relation to three-dimensional flow is used to derive the initial total enthalpy profiles from the mean-velocity profiles. Finally, a Van Driest transformation enables the analytic profile representation to be extended to compressible flow. The starting conditions for the calculation are thus completely defined by a few global parameters at each y-station on the initial line. These starting procedures are identical to those used by the earlier method of Johnston,[8,9] to which reference should be made for further details.

The iterative solution procedure can now be summarized. Equation (22) is solved in turn for U, V and H at all grid points along the surface normal at station (i, j). Thereafter, equation (14) is used to update the two streamfunctions Ψ and Φ, the discretization of the streamfunction relations being centred at $(i-1/2, j, k)$. This sequence is repeated for $j=1$ to J and represents one cycle of the iteration procedure. The process is repeated until the solution over the whole yz-plane through x_i has converged. A suitable convergence criterion can be defined in terms of the corrections to the mean-velocity component U:

$$|\delta u_k| < 10^{-5} \quad \text{for all } j, k. \tag{23}$$

In its current form the present calculation method solves the boundary layer equations in direct mode and so will break down in the presence of separated flow. The separation of a three-dimensional boundary layer may be two-dimensional in nature, with the skin friction tending to zero. Alternatively, flow separation can be characterized by a convergence of the limiting surface streamlines, which results in problems in obtaining solution convergence. The present method takes the approach adopted by other direct boundary layer methods, and the solution is not allowed to enter separated flow regions. In practical terms, any station (i_s, j_s) at which U becomes negative somewhere across the boundary layer is marked as separated flow.

Similarly, any stations at which the skin friction is calculated to be zero or negative are also marked as separated flow. No further use is made of information at these separated flow stations. Stations downstream of (i_s, j_s), i.e. (i, j_s) for $i = i_s + 1$ to I, are also assumed to have separated flow. In this way the boundaries of the separated flow region are mapped out as the calculation marches downstream in the x-direction. Grid points adjacent to separated flow regions are treated in the same way as the two lateral boundaries $j=1$ and $j=J$ (see Table II). This means that y-derivatives

are set to zero at points which would require information from inside the separated flow region.

The problem of marching the boundary layer equations into separated flow regions can be overcome using an inverse formulation.[2]

TURBULENCE MODELLING

As noted in the introduction, a major limiting factor on the accuracy of predictions from present-day calculation methods is the poor state of turbulence modelling for three-dimensional boundary layer flows. The measurements of Elsenaar and Boelsma[6] in an infinite swept wing flow illustrate some of the current limitations in turbulence modelling. For a flow driven into three-dimensionality by an imposed pressure distribution, the direction of the shear stress vector lags behind that of the mean-velocity gradient vector. Thus the assumption of an isotropic eddy viscosity μ_t to model the two shear stress terms appearing in the momentum equations (2) and (3) is invalid. This point has been discussed by van den Berg[16] and Rotta,[17] the latter author proposing a non-isotropic eddy viscosity model. However, the model of Rotta is not independent of the adopted co-ordinate system, since it works in terms of velocity components. A second, and perhaps more important, feature of three-dimensional turbulent boundary layers is the smaller than expected levels of shear stresses in regions of large crossflow. By this is meant that the shear stress levels are smaller than those predicted by the straightforward extension of a two-dimensional turbulence model to three-dimensional flow.

Notwithstanding the above discussion, the present calculation method adopts the isotropic eddy viscosity assumption and extends a number of existing 'standard' two-dimensional flow turbulence models to three-dimensional flow applications. An assessment of the accuracy or otherwise of these models can be used as the starting point for investigations aimed at improving predictions for three-dimensional flows. Three levels of turbulence modelling are considered, these being categorized by the number of auxiliary transport equations that have to be solved.

Algebraic model

An algebraic turbulence model requires no additional differential equations to be solved. The Cebeci–Smith model,[18] extended to three-dimensional flow by Cebeci *et al.*,[15] is used by many existing calculation methods. As such, it can be considered as a base-line model against which to assess the more sophisticated transport equation models.

The eddy viscosity distribution is specified in two parts. A mixing length l_m is defined in the inner region of the boundary layer:

$$\mu_{t_i} = R\rho l_m^2 \left[\left(\frac{\partial U}{\partial Z}\right)^2 + \left(\frac{\partial V}{\partial Z}\right)^2 + 2\cos\theta \frac{\partial U}{\partial Z}\frac{\partial V}{\partial Z} \right]^{1/2}, \tag{24}$$

where

$$l_m = f\kappa Z, \qquad \kappa = 0{\cdot}41, \tag{25}$$

f being the Van Driest damping function

$$f = 1 - e^{-Z/A}, \qquad A = \frac{A^+ \mu}{RU_\tau \rho}\left(\frac{\rho}{\rho_w}\right)^{1/2}, \qquad A^+ = 26 \tag{26}$$

and U_τ is the wall friction velocity. The eddy viscosity in the outer part of the boundary layer is given by

$$\mu_{t_o} = C\rho U_{es} R\delta_k^* \gamma, \qquad \gamma = \frac{1}{1 + 5{\cdot}5(Z/\delta)^6}, \tag{27}$$

and represents essentially a constant kinematic eddy viscosity μ_t/ρ modified by the intermittency function γ. δ is the boundary layer thickness and

$$\delta_k^* = \int_0^\infty (1 - U_t/U_{es}) dZ \tag{28}$$

is a kinematic integral thickness. C is a constant which Cebeci *et al.*[15] put equal to 0·0168, in agreement with the formulation for two-dimensional flow. The measurements of Elsenaar and Boelsma[6] indicate that C decreases in regions of strong crossflow, and this point will be returned to in the results section below. Finally, a hyperbolic tangent function is used to ensure a smooth transition from the inner to the outer eddy viscosity formulation:

$$\mu_t = \mu_{t_o} \tanh(\mu_{t_i}/\mu_{t_o}). \tag{29}$$

Two-equation model

The most sophisticated turbulence model implemented in the present calculation method is the low-Reynolds-number k–ε model due to Chien.[19] The two transport equations employed by this model, written in terms of a non-orthogonal surface co-ordinate system, are

k-equation

$$\frac{\rho U}{h_1}\frac{\partial k}{\partial X} + \frac{\rho V}{h_2}\frac{\partial k}{\partial Y} + \rho W \frac{\partial k}{\partial Z} = \frac{\partial}{\partial Z}\left(\frac{\mu + \mu_t/\sigma_k}{R}\frac{\partial k}{\partial Z}\right) + P_k - \rho\varepsilon - k\Phi_k, \tag{30}$$

ε-equation

$$\frac{\rho U}{h_1}\frac{\partial \varepsilon}{\partial X} + \frac{\rho V}{h_2}\frac{\partial \varepsilon}{\partial Y} + \rho W \frac{\partial \varepsilon}{\partial Z} = \frac{\partial}{\partial Z}\left(\frac{\mu + \mu_t/\sigma_\varepsilon}{R}\frac{\partial \varepsilon}{\partial Z}\right) + c_{\varepsilon_1} f_{\varepsilon_1}\frac{\varepsilon}{k}P_k - c_{\varepsilon_2} f_{\varepsilon_2}\rho\frac{\varepsilon^2}{k} - \varepsilon\Phi_\varepsilon, \tag{31}$$

where k is the turbulent kinetic energy and ε is the rate of dissipation of k. P_k is the production term in the k-equation,

$$P_k = \frac{\mu_t}{R}\left[\left(\frac{\partial U}{\partial Z}\right)^2 + \left(\frac{\partial V}{\partial Z}\right)^2\right]. \tag{32}$$

Again, an isotropic eddy viscosity has been assumed and the eddy viscosity relation is

$$\mu_t = c_\mu f_\mu R\rho\, k^2/\varepsilon. \tag{33}$$

The various low-Reynolds-number versions of the k–ε turbulence model proposed in the literature can be distinguished by the forms adopted for the damping functions $f_\mu, f_{\varepsilon_1}, f_{\varepsilon_2}$ and the near-wall terms Φ_k, Φ_ε. For the Chien version of the model these functions and terms take the form

$$\begin{aligned} &\Phi_k = 2\mu/RZ^2, \qquad \Phi_\varepsilon = 2\mu f_\varepsilon/RZ^2, \qquad f_\mu = 1 - e^{-0\cdot0115Z^+}, \\ &f_{\varepsilon_1} = 1, \qquad f_{\varepsilon_2} = 1 - 0\cdot222e^{-(R_T/6)^2}, \qquad f_\varepsilon = e^{-Z^+/2}, \end{aligned} \tag{34}$$

with

$$Z^+ = R\rho U_\tau Z/\mu, \qquad R_T = R\rho k^2/\mu\varepsilon.$$

The definition of the model is completed by specification of the various constants

$$c_\mu = 0\cdot09, \quad \sigma_k = 1\cdot0, \quad \sigma_\varepsilon = 1\cdot3, \quad c_{\varepsilon_1} = 1\cdot37, \quad c_{\varepsilon_2} = 1\cdot8 \tag{35}$$

and boundary conditions

$$k=\varepsilon=0 \quad \text{at } Z=0,$$
$$k=\varepsilon=0 \quad \text{as } Z\to\infty \tag{36}$$

for the k- and ε-equations.

Equations (30) and (31) are treated in the same way as the mean-flow equations and are written in a similar form to equation (9), where

$m=4$ (k-equation)

$$\alpha_4\equiv k, \qquad A_4=0, \qquad B_4=0, \qquad C_4=\Phi_k/\rho,$$
$$b_4=(\mu+\mu_t/\sigma_k)/R, \qquad R_4=P_k/\rho-\varepsilon,$$

$m=5$ (ε-equation)

$$\alpha_5\equiv\varepsilon, \qquad A_5=0, \qquad B_5=0, \qquad C_5=c_{\varepsilon_2}f_{\varepsilon_2}\,\varepsilon/k+\Phi_\varepsilon/\rho,$$
$$b_5=(\mu+\mu_t/\sigma_\varepsilon)/R, \qquad R_5=c_{\varepsilon_1}f_{\varepsilon_1}(\varepsilon/k)\,P_k/\rho.$$

The k- and ε-equations are linearized by evaluating all terms apart from α_m in equation (9) at the previous iteration level. Note that the above choices of C_4, R_4, C_5 and R_5 are not unique. However, the present formulation does not require any special treatment of the production and destruction terms to achieve a stable solution to the discretized k- and ε-equations. This can be contrasted with the approach taken by the original method of Johnston,[7] in which special procedures were needed to remove step length limitations on the solution of the discretized turbulence transport equations.

One-equation model

The one-equation turbulence model implemented in the present calculation method is based on that used by Hassid and Poreh[20] and Johnston[21] in two-dimensional flows. Equation (30), in an identical form to that used in the Chien k–ε model, is solved for the turbulent kinetic energy k. The dissipation rate ε is determined via an algebraically defined dissipation length scale L_ε:

$$\varepsilon=\frac{f_\varepsilon k^{3/2}}{L_\varepsilon}, \qquad L_\varepsilon=\frac{0{\cdot}085\delta}{0{\cdot}164}\tanh\left(\frac{\kappa Z}{0{\cdot}085\delta}\right), \tag{37}$$

with

$$f_\varepsilon=1-\mathrm{e}^{-0{\cdot}01189R_Z}, \qquad R_Z=\frac{R\rho k^{1/2}Z}{\mu}. \tag{38}$$

The damping function in the eddy viscosity relation, equation (33), is given by

$$f_\mu=f_\varepsilon^2, \tag{39}$$

and the two constants take the values $c_\mu=0{\cdot}09$ and $\sigma_k=1{\cdot}0$.

Starting profiles of the turbulent kinetic energy k must be provided at all stations on the initial line for both the one-equation k–L_ε model and the two-equation k–ε model. These are determined from eddy viscosity profiles generated by the Cebeci–Smith algebraic turbulence model. Assuming an isotropic eddy viscosity, the local total shear stress τ within the boundary layer is given by

$$\tau=\frac{\mu_t}{R}\left[\left(\frac{\partial U}{\partial Z}\right)^2+\left(\frac{\partial V}{\partial Z}\right)^2+2\cos\theta\,\frac{\partial U}{\partial Z}\frac{\partial V}{\partial Z}\right]^{1/2}. \tag{40}$$

The local turbulent kinetic energy is assumed to be related to τ via the turbulence structural parameter a_1:

$$\tau = a_1 \rho k, \tag{41}$$

where a_1 will be assumed to be constant across the boundary layer. The initial profiles of k are generated using a constant value of a_1 equal to 0·3, in agreement with two-dimensional boundary layer data. However, it should be noted that the measurements of Elsenaar and Boelsma[6] indicate that $a_1 < 0{\cdot}3$ if the flow is significantly three-dimensional.

Initial profiles of the dissipation rate ε required by the k–ε turbulence model are generated using equation (37) of the one-equation model. Finally, the convergence criterion given in equation (23) is supplemented by

$$|\delta k_k| < 10^{-5} \quad \text{for all } j, k, \tag{42}$$

where δk_k is the correction to the turbulent kinetic energy, defined in equation (21).

RESULTS

There is still a relative lack of detailed experimental measurements in fully three-dimensional turbulent boundary layers. The majority of experiments consider quasi-three-dimensional flows so as to reduce the quantity of data to be acquired. The initial validation of the present calculation method will therefore be restricted to a consideration of two of these quasi-three-dimensional flows. However, the two experiments do involve detailed mean-flow and, in one case, turbulence measurements in the boundary layers at a number of stations. The results are presented below in terms of a co-ordinate system comprising the local external flow streamlines and their orthogonal projections. Thus U_s and U_c are the local mean-velocity components, within the boundary layer, in the external streamline (streamwise) and orthogonal (cross-stream) directions respectively.

NLR infinite swept wing experiment

The NLR experiment simulates the incompressible flow over a 35° infinite swept wing. In particular, an initially two-dimensional boundary layer on a planar surface develops into three-dimensionality under the influence of an adverse pressure distribution induced by a body suspended above the surface. Mean-velocity profile data[22] and measurements of all the Reynolds stress components[6] are available for this experiment. Figure 2 shows the external flow data, which have been smoothed and interpolated onto 73 equally spaced X-stations for the calculations. Both the surface pressure coefficient C_p and the external streamline angle α (measured relative to the local X-direction) are specified as boundary conditions. This case has been calculated assuming the flow to be invariant in the Y-direction (see Figure 1), but the experiment does depart from infinite swept wing conditions at the more downstream stations.

Predictions using the standard Cebeci–Smith algebraic turbulence model are compared with experiment in Figure 3. The two mean-velocity components are well predicted up to $X = 0{\cdot}92$ m, but the magnitude of the cross-stream velocity is much too low at stations further downstream. Also, the calculated flow remains fully attached, whereas surface oil-flow visualization indicated flow separation (surface flow completely in the Y-direction) downstream of $X = 1{\cdot}3$ m in the experiment. Although the present calculation uses a direct mode scheme, van den Berg[3] indicates that the presence of the flow separation in the experiment does not make such a calculation unduly sensitive, at least in the region upstream of the immediate vicinity of separation. Similarly, calculations by Abid *et al.*[23] using a non-isotropic eddy viscosity model show little improvement

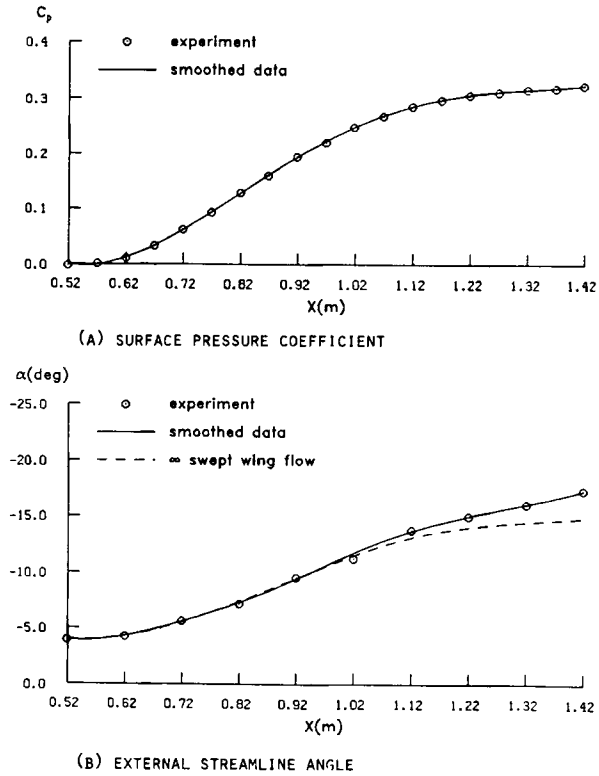

Figure 2. External flow conditions for NLR swept wing experiment

in mean-flow quantities over results with an isotropic eddy viscosity. For these reasons, the level of agreement with experiment shown in Figure 3, when using the standard Cebeci–Smith turbulence model, is consistent with other independent calculations of this flow.[24]

The poor prediction of the mean-velocity profile development downstream of $X = 0{\cdot}92$ m appears to be due to an overprediction of shear stress levels by the Cebeci–Smith model (see Figures 3(c) and 3(d)). In fact, the measurements of Elsenaar and Boelsma[6] indicate that the constant C in equation (27) of the outer eddy viscosity formulation falls significantly below the two-dimensional value of 0·0168. Following Johnston,[9] C is made functionally dependent upon a measure of the flow three-dimensionality, the limiting surface streamline angle β_w being a convenient choice:

$$C = \max\,[0{\cdot}0084,\, 0{\cdot}0168 - 0{\cdot}016\,|\beta_w|]. \tag{43}$$

Figure 3 shows that the predictions are dramatically improved when this modification is incorporated into the standard Cebeci–Smith model. The two mean-velocity components and the streamwise shear stress now agree very well with experiment up to $X = 1{\cdot}22$ m. Also, separation is predicted just downstream of this station, which is a little upstream of the position indicated by experiment. The cross-stream shear stress levels are still too high, but the use of a non-isotropic eddy viscosity will presumably improve these.

Predictions for this case using the one-equation and two-equation turbulence models are shown in Figures 4 and 5 respectively. The one-equation model gives results very similar to those of the

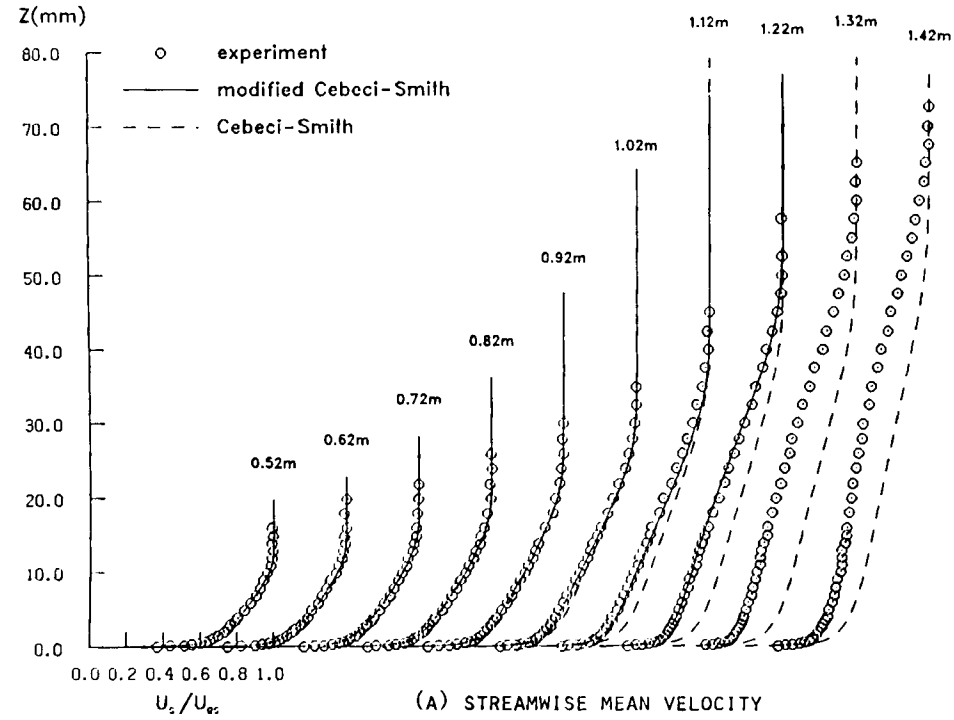

Figure 3(a). Algebraic turbulence model results for NLR experiment

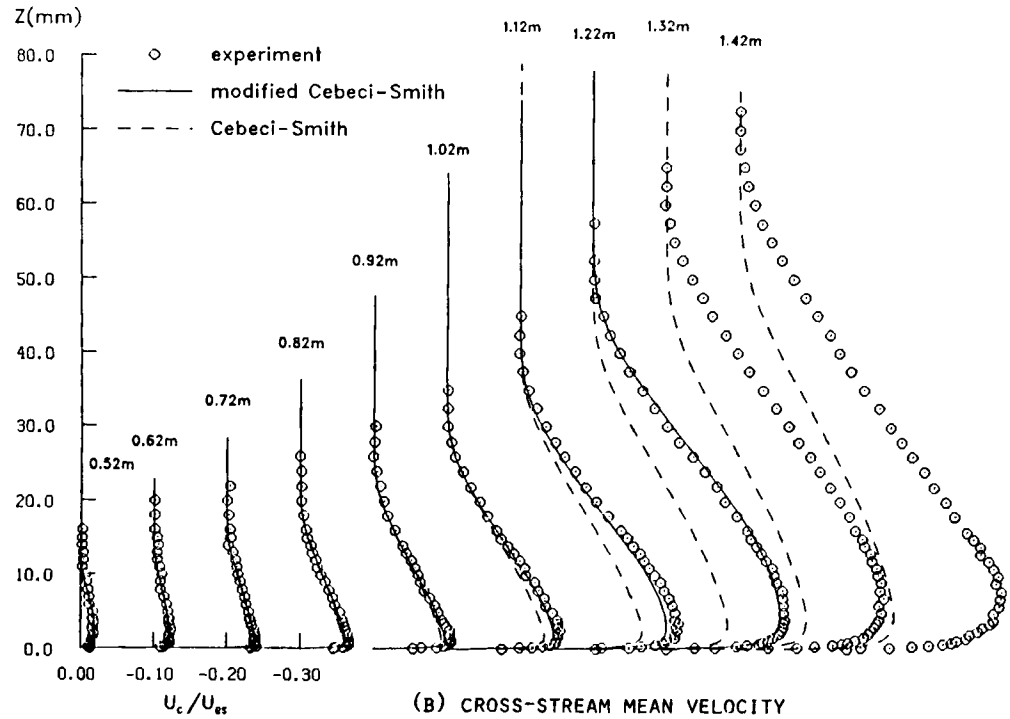

Figure 3(b). Algebraic turbulence model results for NLR experiment

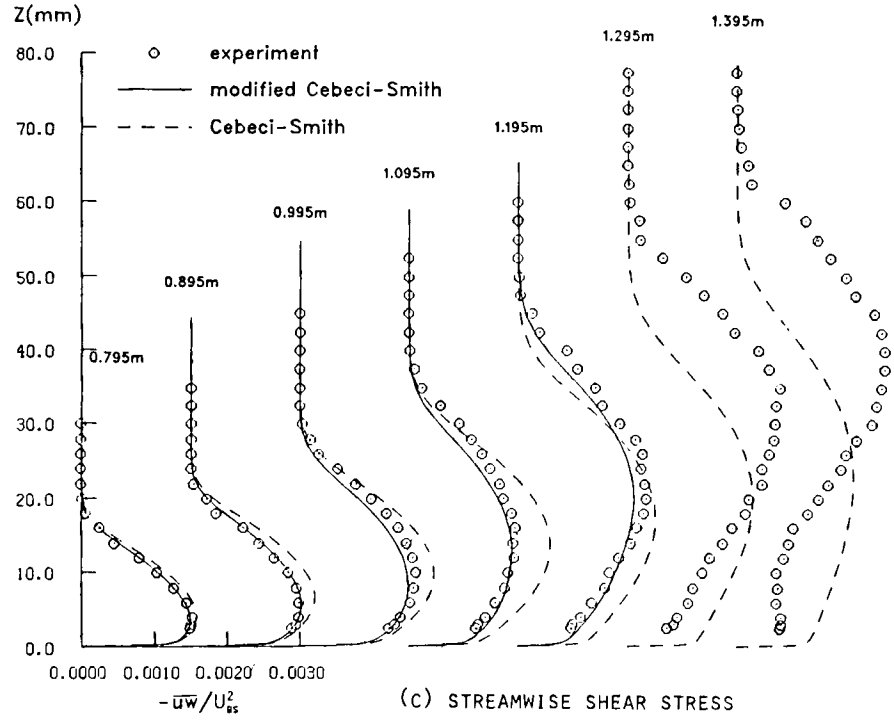

Figure 3(c). Algebraic turbulence model results for NLR experiment

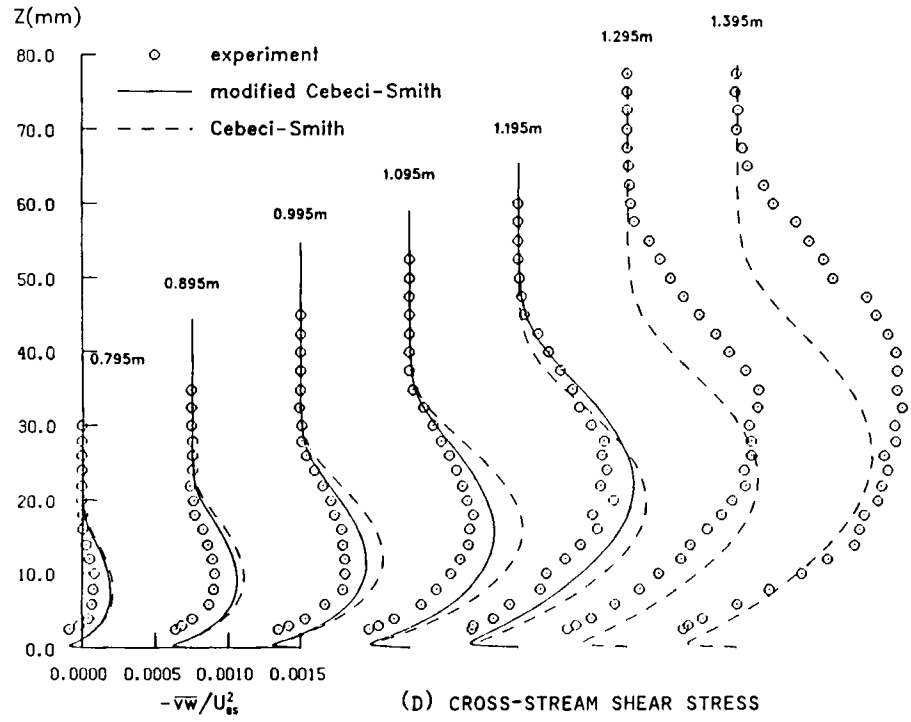

Figure 3(d). Algebraic turbulence model results for NLR experiment

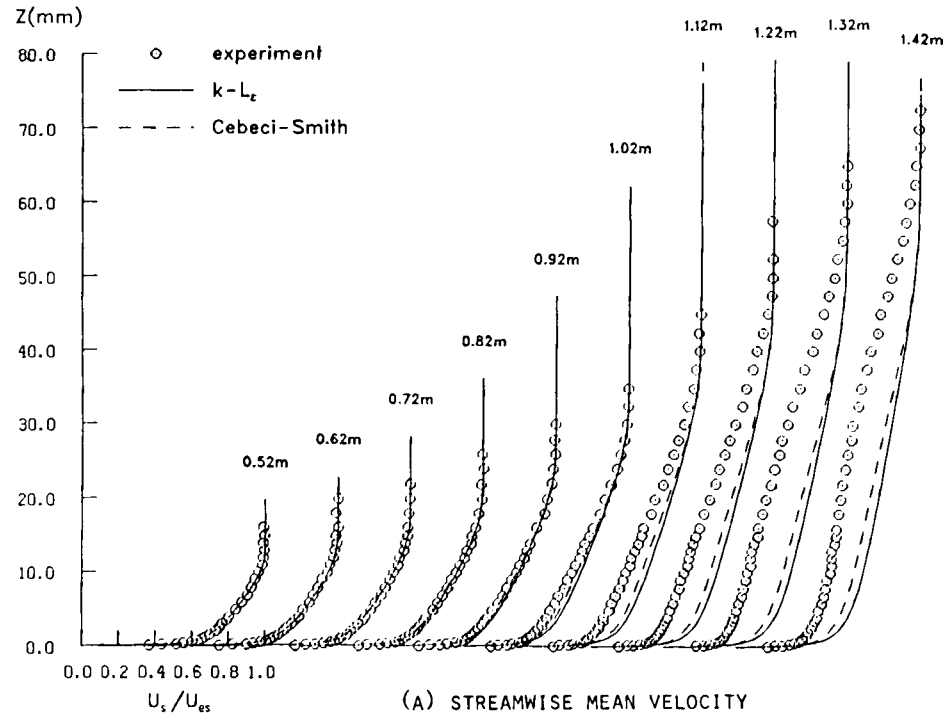

Figure 4(a). One-equation turbulence model results for NLR experiment

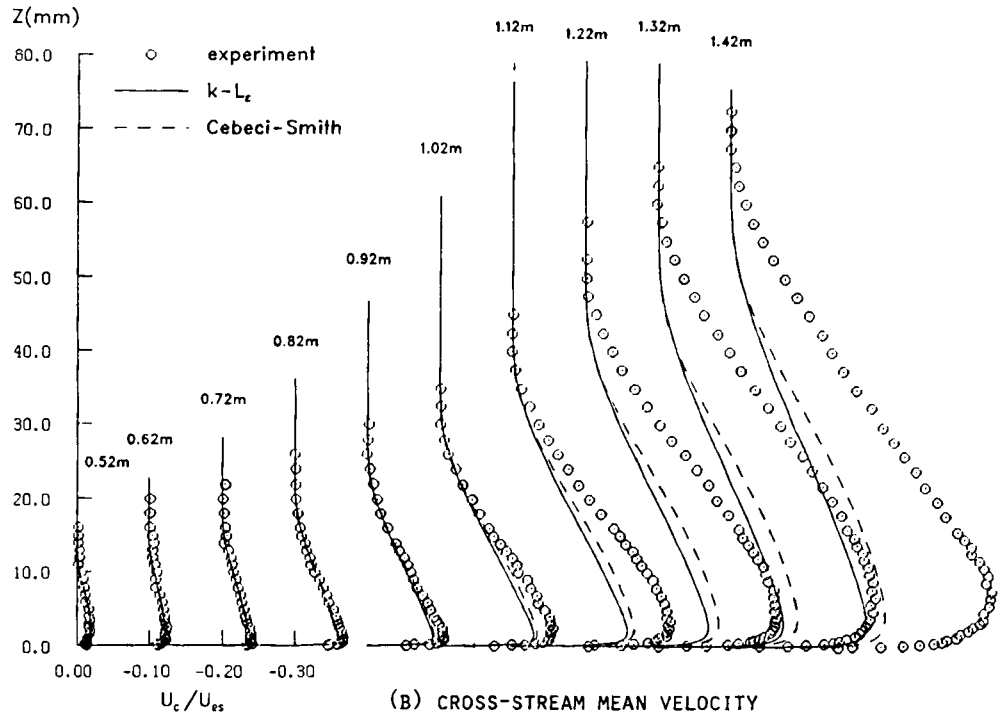

Figure 4(b). One-equation turbulence model results for NLR experiment

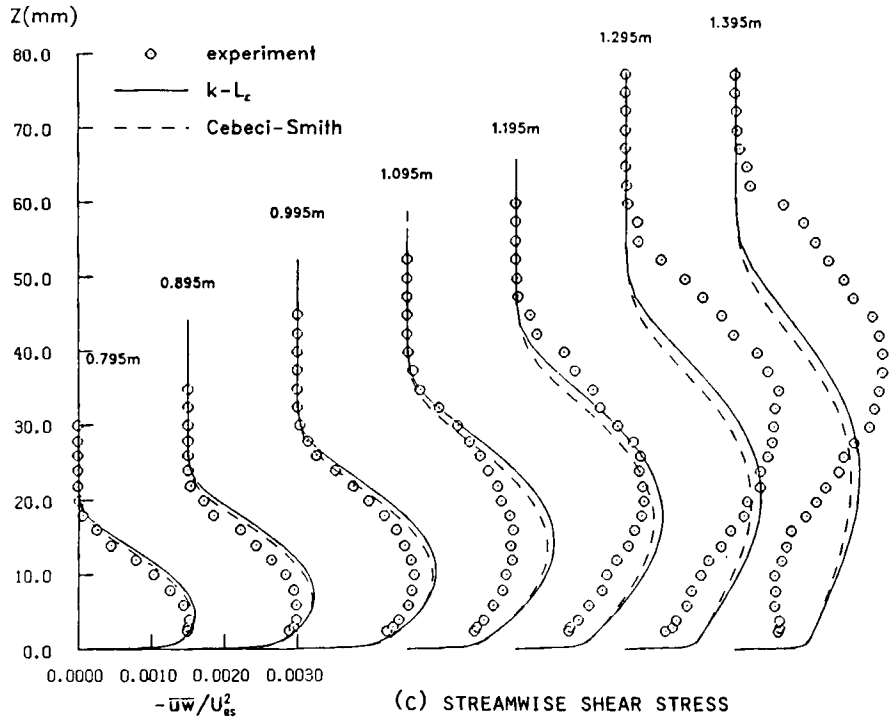

Figure 4(c). One-equation turbulence model results for NLR experiment

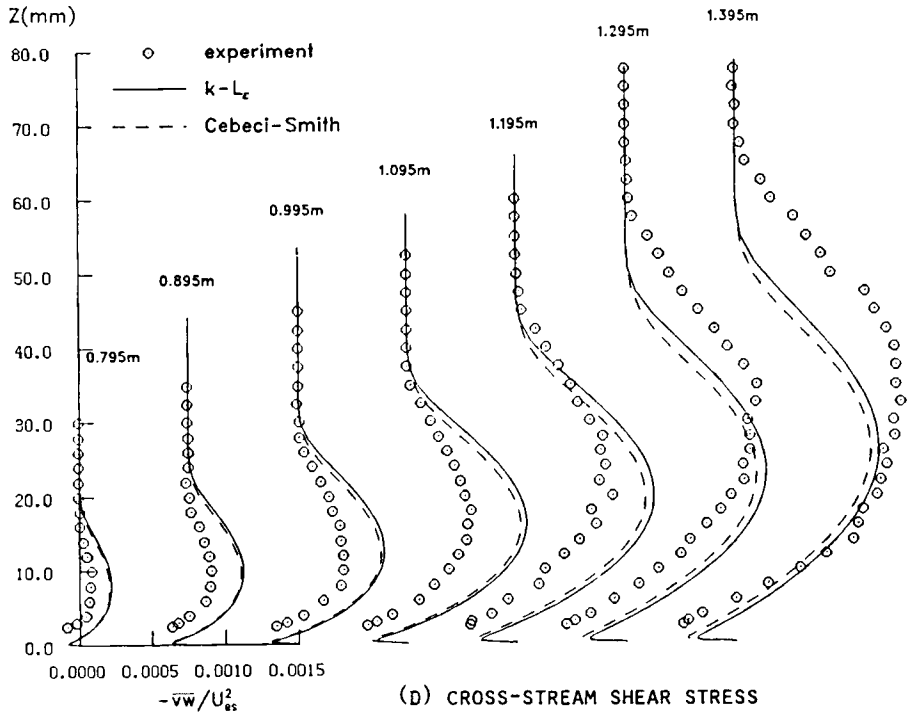

Figure 4(d). One-equation turbulence model results for NLR experiment

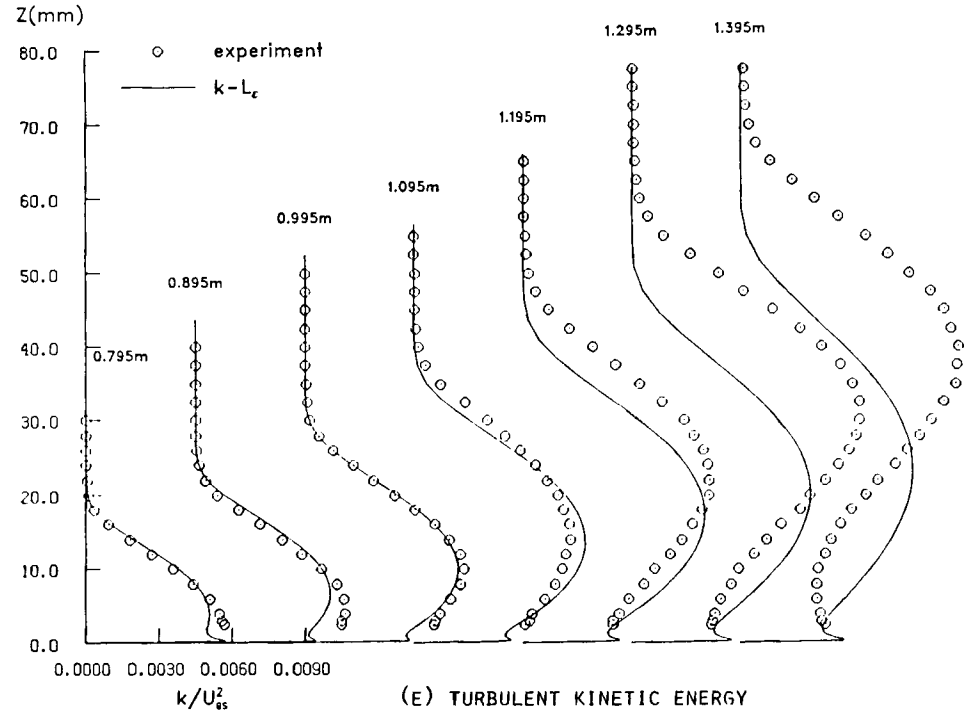

Figure 4(e). One-equation turbulence model results for NLR experiment

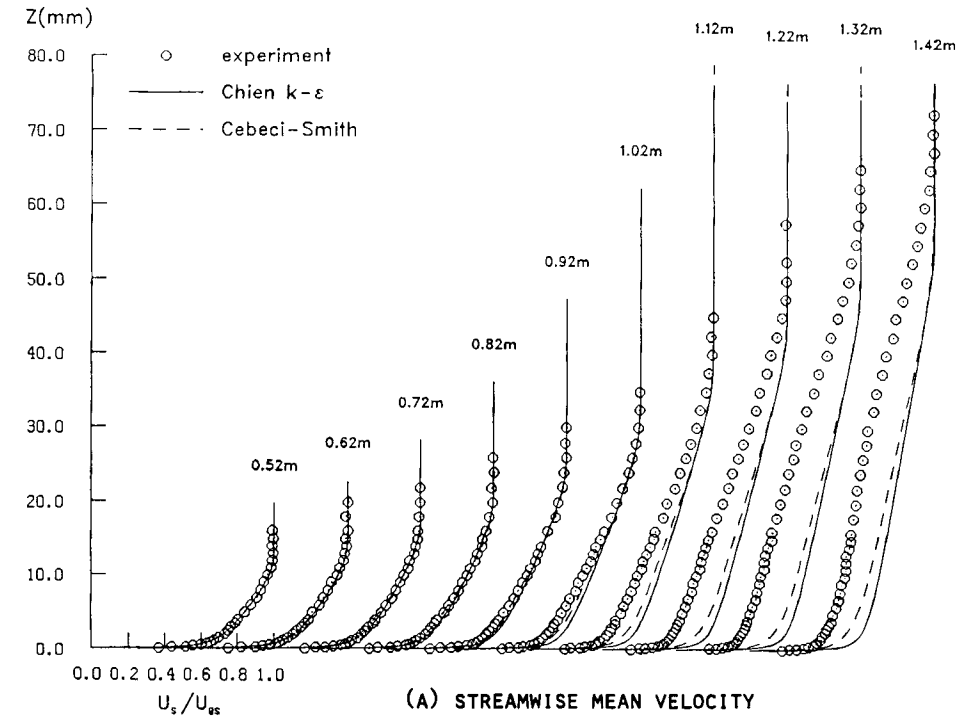

Figure 5(a). Two-equation turbulence model results for NLR experiment

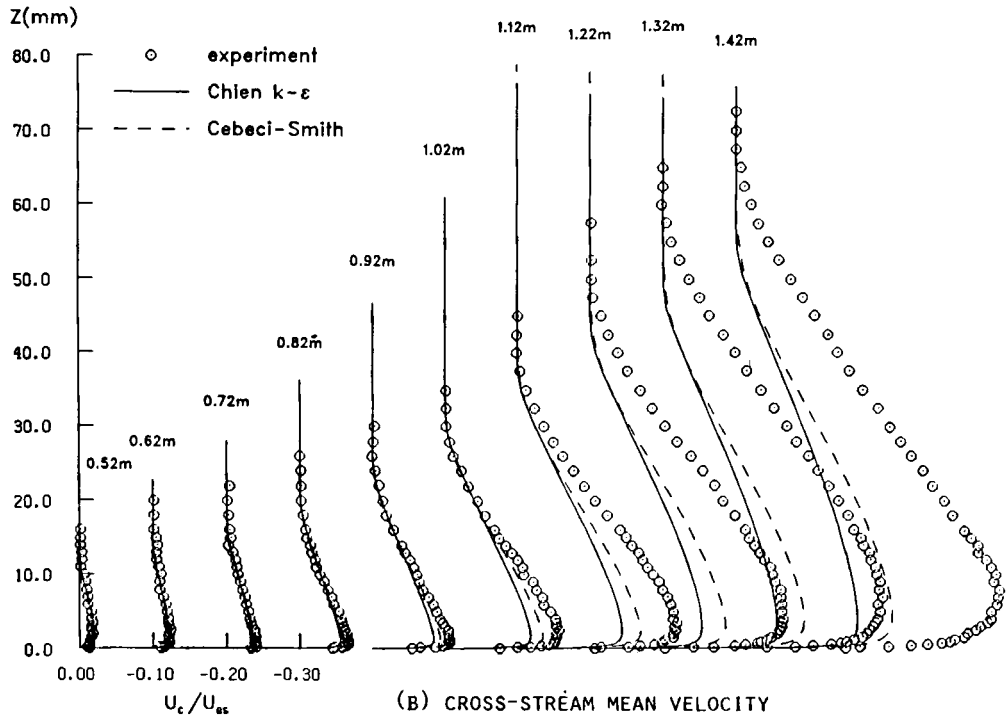

Figure 5(b). Two-equation turbulence model results for NLR experiment

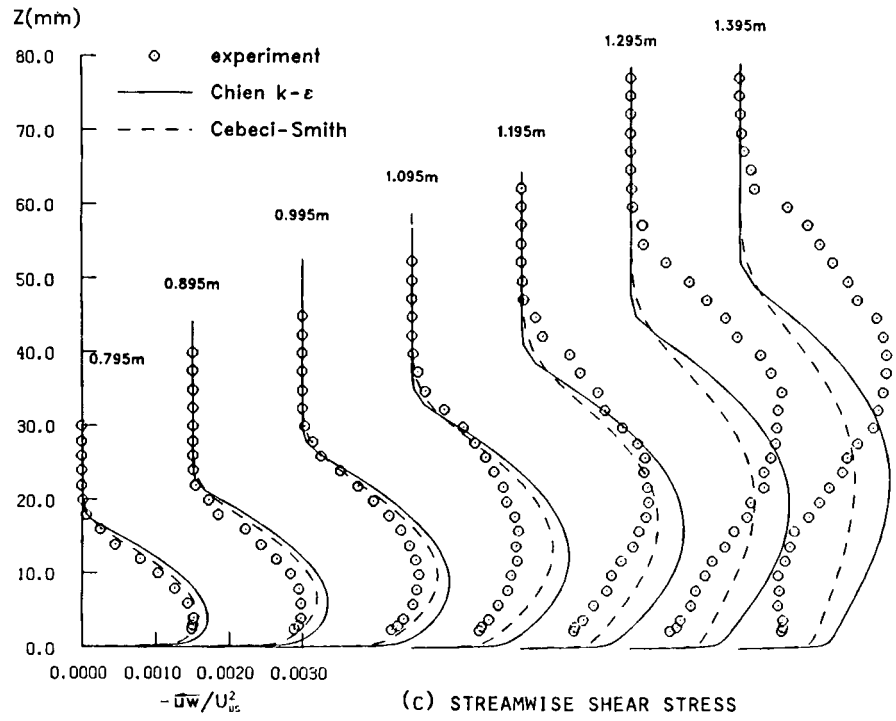

Figure 5(c). Two-equation turbulence model results for NLR experiment

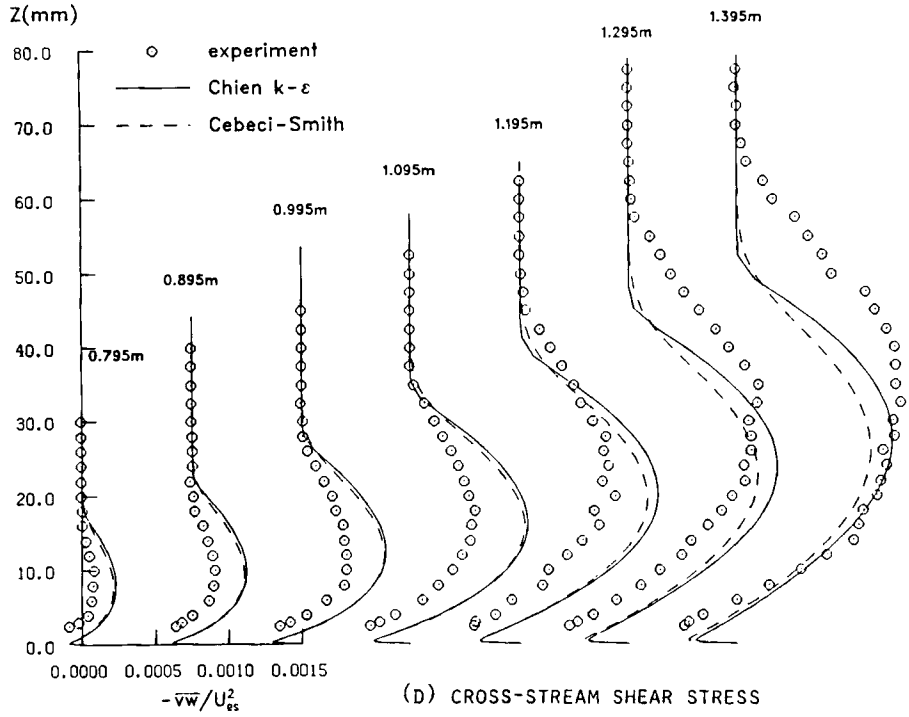

Figure 5(d). Two-equation turbulence model results for NLR experiment

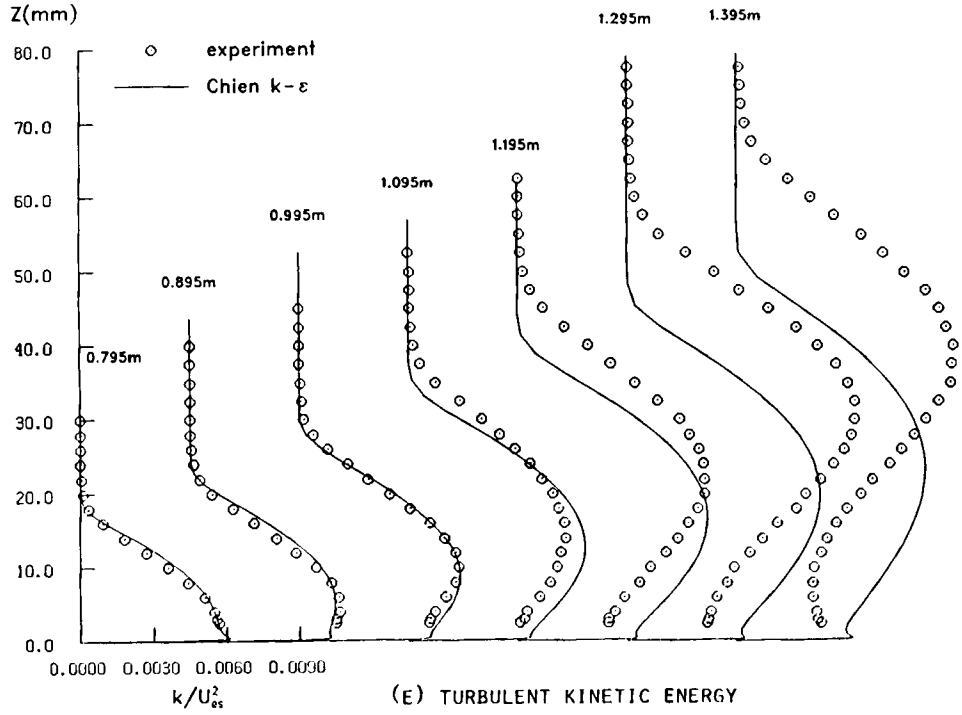

Figure 5(e). Two-equation turbulence model results for NLR experiment

standard Cebeci–Smith model, although the underprediction of the cross-stream mean velocities at the more downstream stations is a little worse. There is a further deterioration in the predictions of cross-stream mean velocities with the two-equation turbulence model. The most probable cause for this is the overprediction of the streamwise shear stress levels in the inner region of the boundary layer compared to the Cebeci–Smith model. The two transport equation turbulence models give good predictions of the turbulent kinetic energy at stations upstream of $X = 1$ m, this being particularly true for the two-equation model.

In conclusion, there are no benefits in using the more sophisticated turbulence models for this case, at least with the models in their current form.

RAE delta wing experiment

The second case to be considered is the delta wing experiment of East.[25] Figure 6 shows the model geometry, which consists of a half-delta wing with a leading edge sweep angle of 76° (semi-apex angle $\bar{\theta} = 14°$) and a root chord of 7·3 m. The flow is incompressible with a free stream velocity of 60 m s^{-1}, and the wing is at an incidence angle of 8°. The experimental data include mean-velocity profiles at a number of stations along a spanwise line inclined 8° to the tunnel floor and at a root chord station 5·53 m downstream of the apex.

The flow is calculated using a surface grid consisting of rays through the apex and lines parallel to the measurement plane, with 35×107 grid points in the spanwise and chordwise directions respectively. Calculations start at a station 2 m upstream of the measurement plane and cover the region $0{\cdot}296 \leqslant \theta/\bar{\theta} \leqslant 0{\cdot}804$, which is between the attachment line ($\theta/\bar{\theta} \approx 0{\cdot}18$) and the secondary separation line ($\theta/\bar{\theta} \approx 0{\cdot}825$). Conical flow conditions are assumed and the external flow distributions shown in Figure 7 are imposed at all chordwise stations. Starting conditions on the initial line are generated rather crudely[9] following the recommendations of East.[24]

The present calculations use the second-order-accurate upwind scheme for y-derivatives in the convective transport terms; see equation (19) and Table II(a). Experience with the earlier method of Johnston[9] indicates that the QUICK scheme gives essentially identical results for this case.

Figure 8 compares predictions using the Cebeci–Smith turbulence model with experiment. The boundary layer thins in the spanwise y-direction under the influence of the primary vortex flow field. The cross-stream mean-velocity component is overpredicted in the favourable spanwise

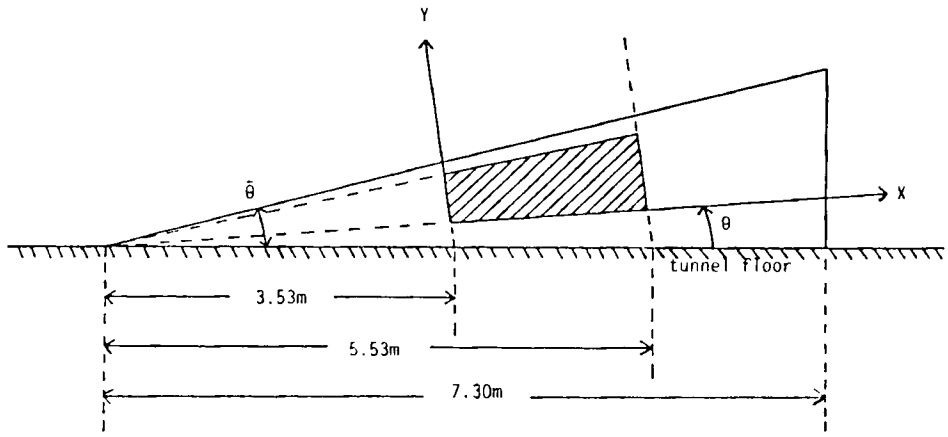

Figure 6. Model geometry for RAE delta wing experiment

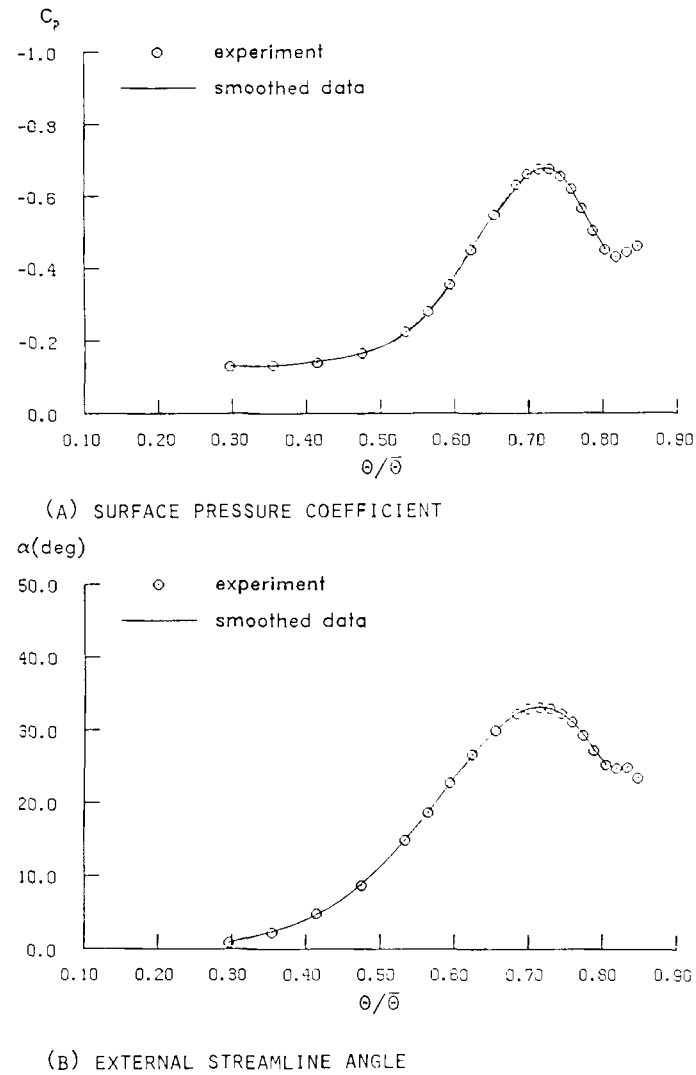

Figure 7. External flow conditions for RAE experiment

pressure gradient region, $\theta/\bar{\theta} < 0{\cdot}7$, and the boundary layer thickness is underpredicted. There is also a significant overprediction of the limiting surface streamline angle β_w in the region near $\theta/\bar{\theta} = 0{\cdot}7$. The modification to the standard Cebeci–Smith model given in equation (43) has a small but adverse effect on the predictions. At the more outboard stations the spanwise pressure distribution becomes adverse. This results in negative cross-stream mean velocities in the boundary layer, but the magnitude of these is considerably underpredicted. However, the boundary layer is approaching separation in this region and there is likely to be a strong interaction between the inner viscous and outer inviscid flow fields. Also, East[25] calculates the cross-stream eddy viscosities to be only 40% of the corresponding streamwise values. Further, poor predictions by the Cebeci–Smith model of boundary layer development in favourable pressure gradient conditions have also been noted in two-dimensional flow situations.[21]

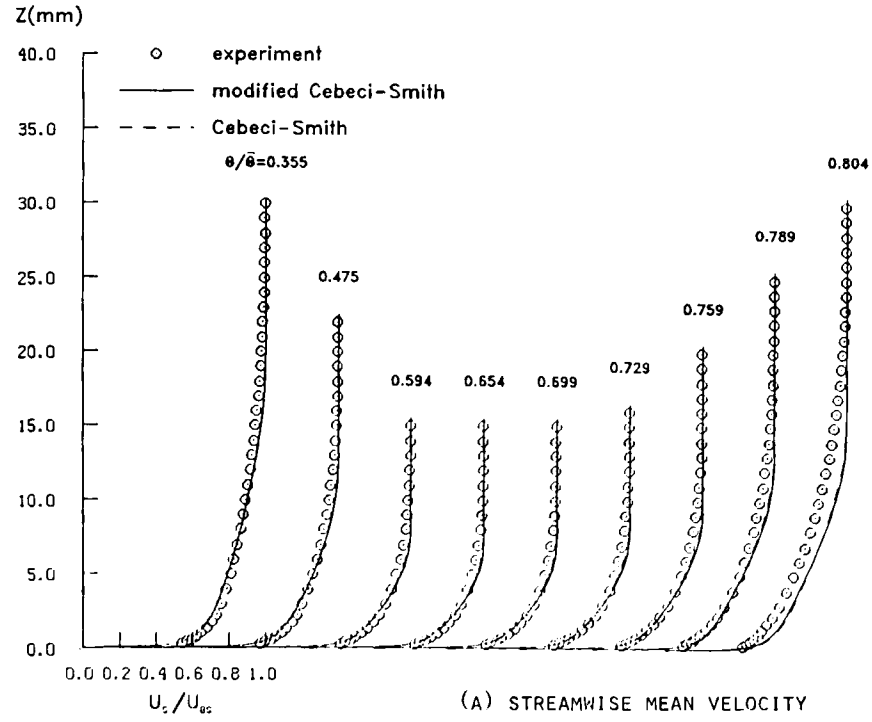

Figure 8(a). Algebraic turbulence model results for RAE experiment

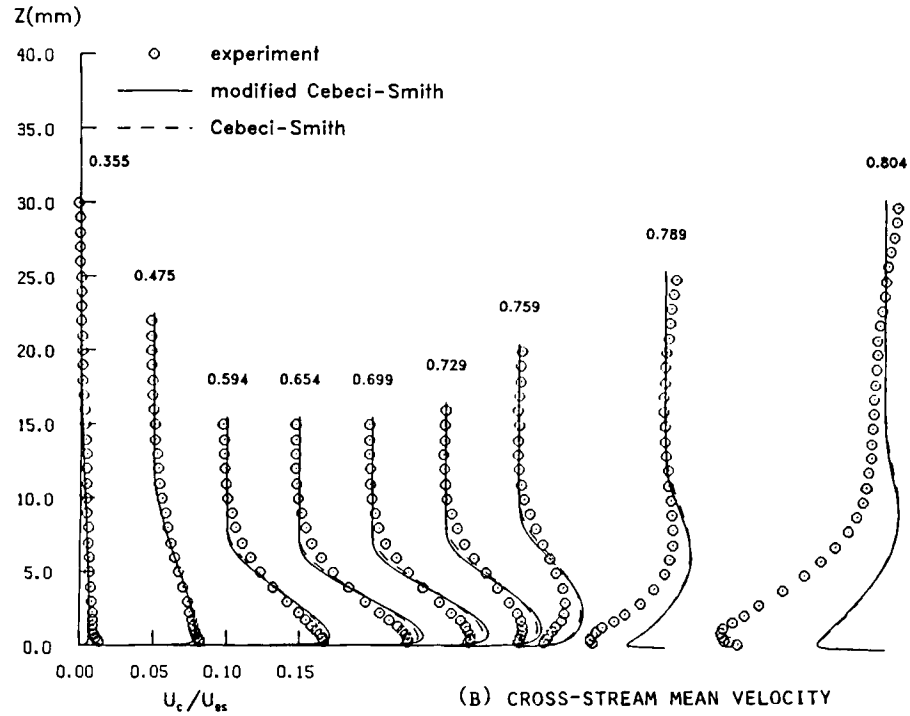

Figure 8(b). Algebraic turbulence model results for RAE experiment

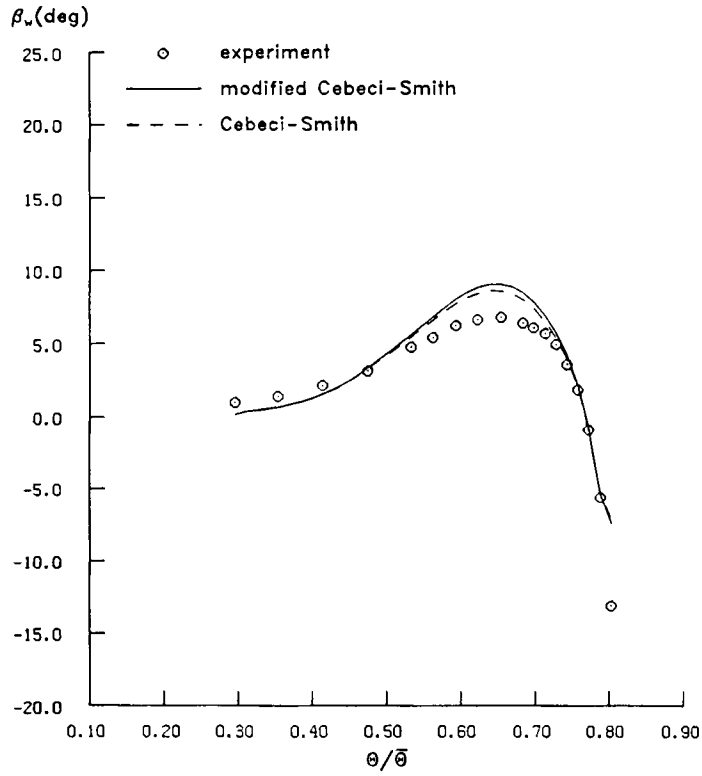

(c) LIMITING SURFACE STREAMLINE ANGLE

Figure 8(c). Algebraic turbulence model results for RAE experiment

Figure 9 indicates only relatively minor improvements when the one-equation model is used. In contrast, the results from the two-equation model, Figure 10, are in substantially better agreement with experiment in the favourable pressure gradient region. The boundary layer thickness, cross-stream mean-velocity profile and limiting surface streamline angle are all well predicted for $\theta/\bar{\theta} < 0{\cdot}7$. There is, however, no improvement in results for the adverse pressure gradient region further outboard.

Typical computer CPU times for the present calculation method are as follows: 0·774 s with the Cebeci–Smith algebraic turbulence model, 0·962 s using the one-equation model and 2·596 s for the two-equation model. These figures relate to computation time per surface station (with 65 grid points across the boundary layer) for the RAE delta wing case on a VAX 11/780 computer.

CONCLUSIONS

An efficient method to solve the three-dimensional turbulent boundary layer equations has been developed. The method is applicable to the compressible flow development over general developable surfaces by use of a curvilinear surface co-ordinate system. The governing mean-flow and, if applicable, turbulence transport equations are solved in finite difference form. In particular, upwind formulae are used to discretize the convective transport terms appearing in the equations. A consistent approach is taken to the discretization and linearization of the various equations by

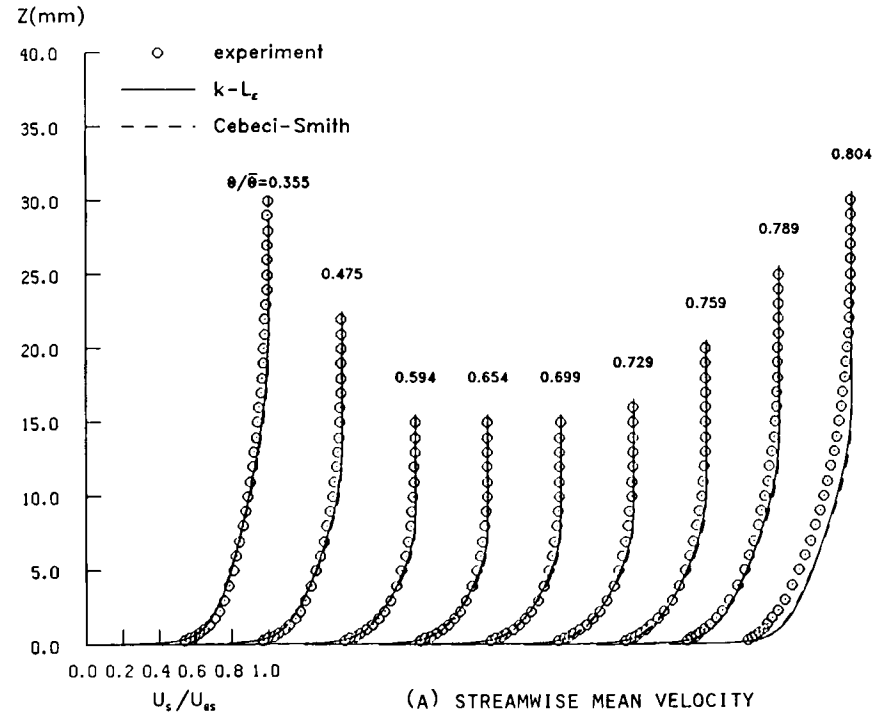

Figure 9(a). One-equation turbulence model results for RAE experiment

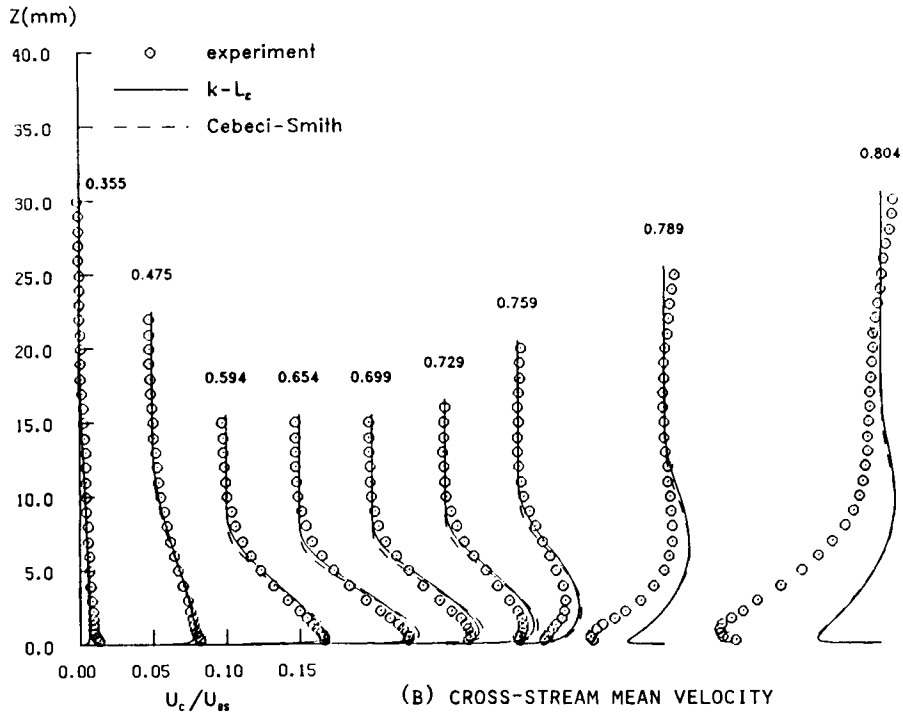

Figure 9(b). One-equation turbulence model results for RAE experiment

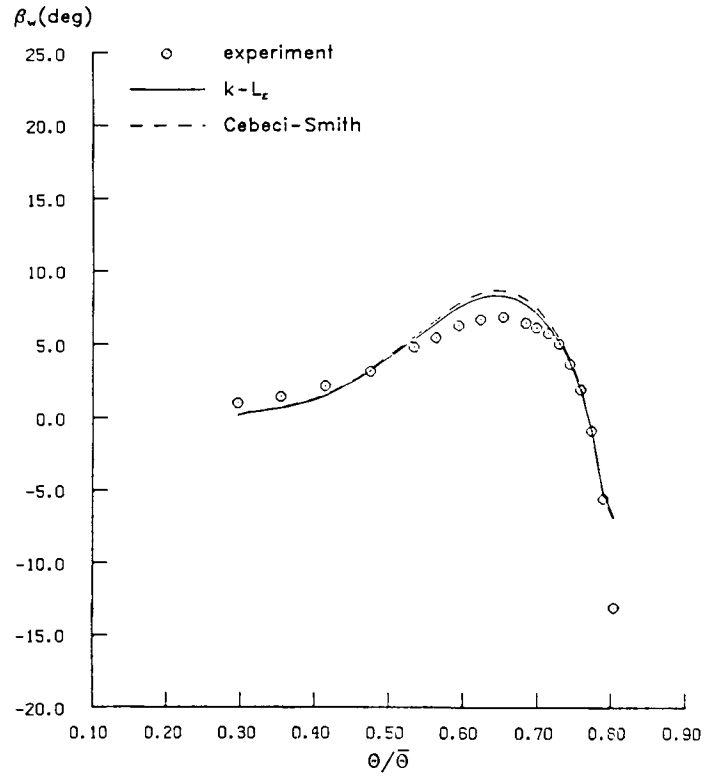

Figure 9(c). One-equation turbulence model results for RAE experiment

casting them all in a similar form. The implementation of algebraic, one-equation and two-equation turbulence models has been described. Calculations using all three turbulence models have been presented for two quasi-three-dimensional flow experiments.

Detailed comparisons of predicted and measured mean-velocity and, in one case, shear stress profiles enable a number of preliminary conclusions to be made. The algebraic Cebeci–Smith model and a one-equation model, which solves the turbulent kinetic energy equation, give essentially the same results for the two cases considered. The two-equation turbulence model performs better for flows involving favourable pressure gradients. However, the performance of this model is inferior to the algebraic and one-equation models in adverse pressure gradient conditions.

The present, albeit rather limited, evaluation indicates some of the more obvious deficiencies in the current state of the art as regards turbulence modelling for three-dimensional boundary layers. One main objective of the development of the present calculation method has been to provide a vehicle within which improvements to these 'standard' turbulence models can be investigated in a consistent way. Also, the use of a general discretization of the crossflow convective transport terms in the flow equations enables various proposals for approximating these important terms to be assessed. Finally, a version of the present method which solves the governing equations in inverse mode is desirable to allow the calculations to proceed into separated flow regions.

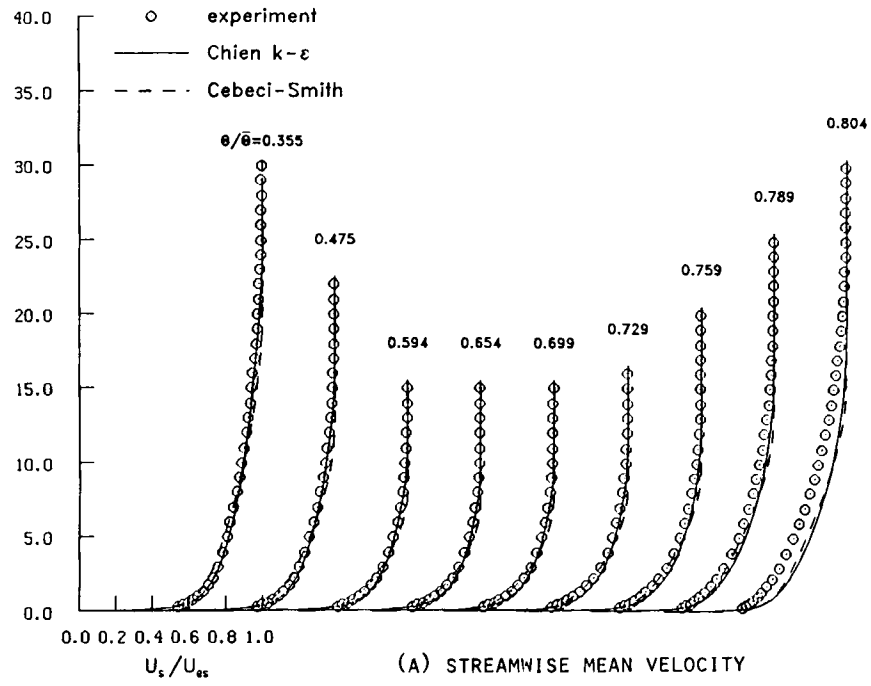

Figure 10(a). Two-equation turbulence model results for RAE experiment

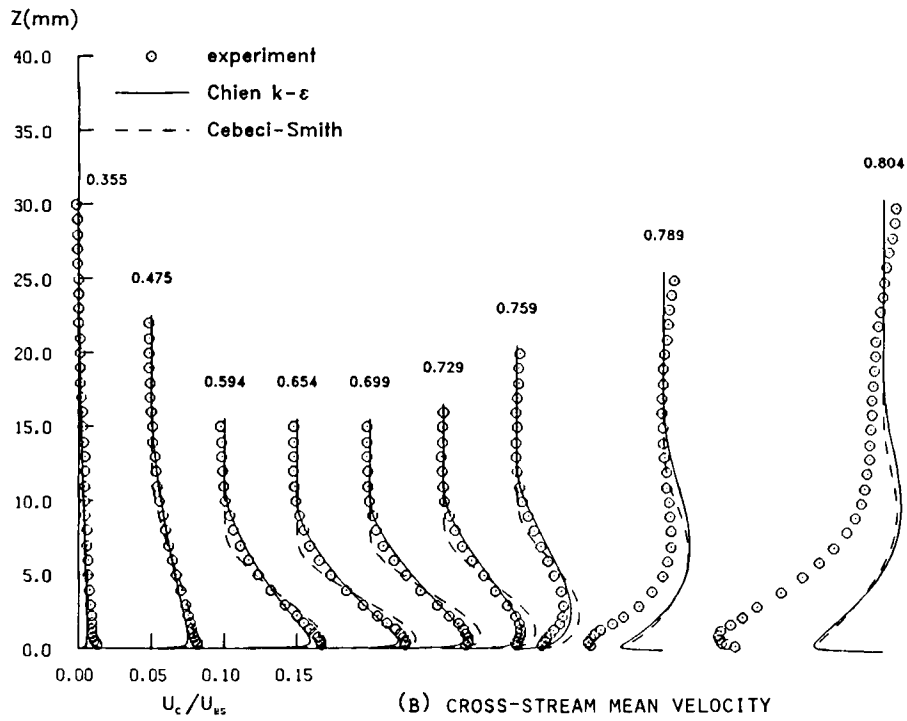

Figure 10(b). Two-equation turbulence model results for RAE experiment

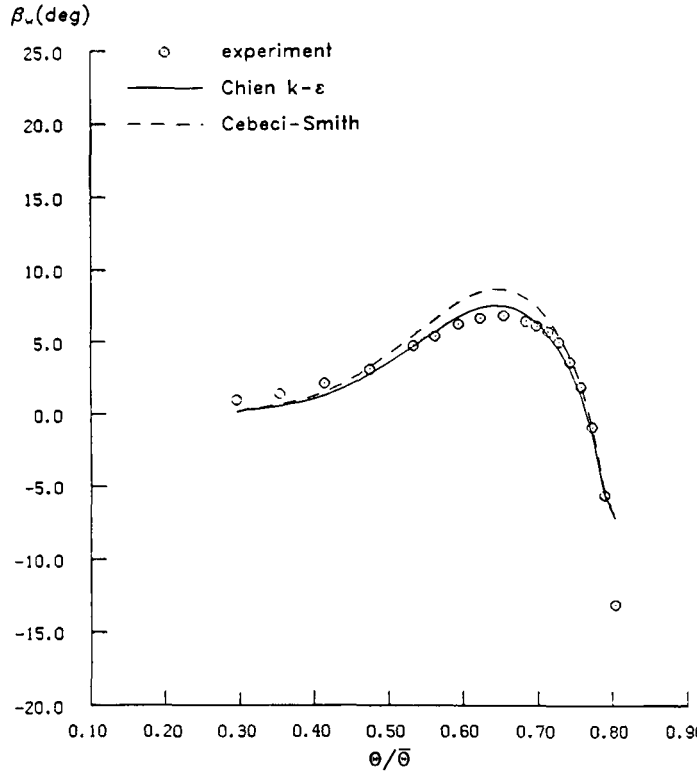

Figure 10(c). Two-equation turbulence model results for RAE experiment

APPENDIX

The boundary layer equations are solved in a curvilinear co-ordinate system consisting of two non-orthogonal surface co-ordinates X and Y with an angle θ between them (Figure 1). The third co-ordinate Z is in a direction normal to the surface. The surface itself is defined in terms of Cartesian co-ordinates $(\bar{X}, \bar{Y}, \bar{Z})$, the transformation between the two surface co-ordinate systems being given by

$$\bar{X}=g_1(X, Y), \qquad \bar{Y}=g_2(X, Y), \qquad \bar{Z}=g_3(X, Y).$$

In general, the functions g_1 to g_3 will not be known analytically. If ds is an element of length on the surface, then

$$ds^2=d\bar{X}^2+d\bar{Y}^2+d\bar{Z}^2=h_1^2dX^2+h_2^2dY^2+2h_1h_2\cos\theta dX dY,$$

with

$$h_1^2=\left(\frac{\partial g_1}{\partial X}\right)^2+\left(\frac{\partial g_2}{\partial X}\right)^2+\left(\frac{\partial g_3}{\partial X}\right)^2,$$

$$h_2^2=\left(\frac{\partial g_1}{\partial Y}\right)^2+\left(\frac{\partial g_2}{\partial Y}\right)^2+\left(\frac{\partial g_3}{\partial Y}\right)^2,$$

$$h_1h_2\cos\theta=\frac{\partial g_1}{\partial X}\frac{\partial g_1}{\partial Y}+\frac{\partial g_2}{\partial X}\frac{\partial g_2}{\partial Y}+\frac{\partial g_3}{\partial X}\frac{\partial g_3}{\partial Y}.$$

The following metric quantities are also required:

$$k_1 = \frac{1}{h_1 h_2 \sin\theta}\left(\frac{\partial(h_2\cos\theta)}{\partial X} - \frac{\partial h_1}{\partial Y}\right),$$

$$k_2 = \frac{1}{h_1 h_2 \sin\theta}\left(\frac{\partial(h_1\cos\theta)}{\partial Y} - \frac{\partial h_2}{\partial X}\right),$$

$$k_{12} = \frac{1}{\sin\theta}\left[\cos\theta\left(k_2 + \frac{1}{h_2}\frac{\partial\theta}{\partial Y}\right) - \left(k_1 + \frac{1}{h_1}\frac{\partial\theta}{\partial X}\right)\right],$$

$$k_{21} = \frac{1}{\sin\theta}\left[\cos\theta\left(k_1 + \frac{1}{h_1}\frac{\partial\theta}{\partial X}\right) - \left(k_2 + \frac{1}{h_2}\frac{\partial\theta}{\partial Y}\right)\right].$$

The various derivatives appearing in the above equations are evaluated numerically using finite difference formulae.

The mean-velocity profiles presented in the results section are plotted in terms of a co-ordinate system comprising the external flow streamlines and their orthogonal projections. U_s and U_c are the local mean-velocity components within the boundary layer in these two directions. The limiting streamline angle at the surface, β_w, is defined relative to the local external streamline angle α:

$$\beta_w = \tan^{-1}[(\partial U_c/\partial Z)/(\partial U_s/\partial Z)]_w.$$

The wall shear stress τ_w is given by

$$\tau_w = \rho_w U_\tau^2 = \frac{\mu_w}{R}\left[\left(\frac{\partial U}{\partial Z}\right)^2 + \left(\frac{\partial V}{\partial Z}\right)^2 + 2\cos\theta\frac{\partial U}{\partial Z}\frac{\partial V}{\partial Z}\right]_w^{1/2}.$$

Finally, the two principal Reynolds shear stresses in the external streamline co-ordinate system are

$$-\rho\overline{uw} = \frac{\mu_t}{R}\frac{\partial U_s}{\partial Z}, \qquad -\rho\overline{vw} = \frac{\mu_t}{R}\frac{\partial U_c}{\partial Z}.$$

REFERENCES

1. U. Kaynak and J. Flores, 'Advances in the computation of transonic separated flows over finite wings', *AIAA Paper 87-1195*, 1987.
2. J. M. Delery and M. J. Formery, 'A finite difference method for inverse solutions of 3D turbulent boundary layer flow', *AIAA Paper 83-0301*, 1983 (also *ONERA TP 1983-4*, 1983).
3. B. Van den Berg, 'Computation of three dimensional boundary layers including separation', *AGARD R 741*, February 1987.
4. D. A. Humphreys and J. P. F. Lindhout, 'Calculation methods for 3D turbulent boundary layers', *Prog. Aerospace Sci.*, **25**, 107–129 (1988).
5. B. van den Berg, D. A. Humphreys, E. Krause and J. P. F. Lindhout, *Three-dimensional Turbulent Boundary Layer Calculations and experiments*, Vieweg, Braunschweig, 1988.
6. A. Elsenaar and S. H. Boelsma, 'Measurements of the Reynolds stress tensor in a three dimensional turbulent boundary layer under infinite swept wing conditions', *NLR TR 74095U*, 1974.
7. L. J. Johnston, 'A numerical method for three-dimensional compressible turbulent boundary-layer flows', *Proc. 5th Int. Conf. on Numerical Methods in Laminar and Turbulent Flow*, Montreal, July 1987, Pineridge Press, Swansea, 1987, pp. 1421–1435.
8. L. J. Johnston, 'A calculation method for compressible three-dimensional turbulent boundary-layer flows', *von Karman Institute, Technical Note 167*, July 1988.
9. L. J. Johnston, 'A solution method for the three-dimensional compressible turbulent boundary-layer equations', *Aeronaut. J.*, **93**, 115–131 (1989).

10. P. D. Smith, 'The numerical computation of three dimensional turbulent boundary layers', *IUTAM Symp. on Three Dimensional Turbulent Boundary Layers*, Berlin, March 1982, Springer, Berlin, 1982, pp. 265–285.
11. J. P. F. Lindhout, E. de Boer and B. van den Berg, 'Three dimensional boundary layer calculations on wings, starting from the fuselage', *NLR MP 82060U*, 1982.
12. J. F. Nash and R. M. Scruggs, 'An implicit method for the calculation of three dimensional boundary layers on fuselage configurations', *Sybucon Inc., Report LG76ER0199*, 1976.
13. A. Tassa, E. H. Atta and L. A. Lemmerman, 'A new three dimensional boundary layer calculation method', *AIAA Paper 82-0224*, 1982.
14. B. P. Leonard, 'A survey of finite differences of opinion on numerical muddling of the incomprehensible defective confusion equation', *ASME AMD 34, Finite Element Methods for Convection Dominated Flows*, 1979, pp. 1–17.
15. T. Cebeci, K. Kaups and J. A. Ramsey, 'A general method for calculating three dimensional compressible laminar and turbulent boundary layers on arbitrary wings', *NASA CR 2777*, 1977.
16. B. van den Berg, 'Some notes on three dimensional turbulent boundary layer data and turbulence modeling', *NLR MP 82007U*, 1982.
17. J. C. Rotta, 'A family of turbulence models for three dimensional thin shear layers', *Proc. Symp. on Turbulent Shear Flows*, Pennsylvania State University, April 1977, pp. 10.27–10.34.
18. T. Cebeci and A. M. O. Smith, *Analysis of Turbulent Boundary Layers*, Academic Press, New York, 1974.
19. K.-Y. Chien, 'Predictions of channel and boundary layer flows with a low Reynolds number turbulence model', *AIAA J.*, **20**, 33–38 (1982).
20. S. Hassid and M. Poreh, 'A turbulent energy model for flows with drag reduction', *J. Fluids Eng. (ASME)*, **97**, 234–241 (1975).
21. L. J. Johnston, 'A calculation method for two-dimensional wall bounded turbulent flows', *Aeronaut. J.*, **90**, 174–184 (1986).
22. B. van den Berg and A. Elsenaar, 'Measurements in a three dimensional incompressible turbulent boundary layer in an adverse pressure gradient under infinite swept wing conditions', *NLR TR 72092U*, 1972.
23. R. Abid, J. Delery and R. Schmitt, 'An examination of turbulence models for a separating three dimensional turbulent boundary layer', *ONERA TP 1985-74*, 1985.
24. L. F. East, 'Computation of three-dimensional turbulent boundary layers', *EUROMECH 60*, Trondheim, 1975, *FFA TN AE-1211*, 1975.
25. L. F. East, 'Measurements of the three dimensional incompressible turbulent boundary layer induced on the surface of a slender delta wing by the leading edge vortex', *RAE TR 73141*, 1974.